

¹ Supplementary Materials File

² Alejandro Damian-Serrano, Steven H.D. Haddock, Casey W. Dunn

³ Supplementary Methods

⁴ DAPC optimization: Some taxa have inapplicable states for certain absent characters (such as
⁵ the length of a nematocyst subtype that is not present in a species), which are problematic for
⁶ DAPC analyses. We tackled this by transforming the absent states to zeroes. This approach
⁷ allows us to incorporate all the data, but creates an attraction bias between small character
⁸ states (*e.g.* small tentilla) and absent states (*e.g.* no tentilla). Absent characters are likely to
⁹ be very biologically relevant to prey capture and we believe they should be accounted for
¹⁰ in a predictive approach. We limited the number of linear discriminant functions retained
¹¹ to the number of groupings in each case. We selected the number of principal components
¹² retained using the a-score optimization function (R adegenet::optim.a.score) (Jombart et
¹³ al. 2010) with 100 iterations, which yielded more stable results than the cross validation
¹⁴ function (R adegenet::xval). This optimization aims to find the compromise value with
¹⁵ highest discrimination power with the least overfitting.

¹⁶ In order to explore the correlational structure among continuous characters and among
¹⁷ their evolutionary histories, we used principal component analysis (PCA) and phylogenetic
¹⁸ PCA (Revell 2012). Since the character dataset contains many gaps due to missing characters
¹⁹ and inapplicable states, we carried out these analyses on a subset of species and characters
²⁰ that allowed for the most complete dataset. This was done by removing the terminal filament
²¹ characters (which are only shared by a small subset of species), and then removing species
²² which had inapplicable states for the remaining characters. In addition, we obtained the
²³ correlations between the phylogenetic independent contrasts (Felsenstein 1985) using the
²⁴ package rphylip (Revell and Chamberlain 2014).

25 Supplementary Results

26 *Generating dietary hypotheses using tentillum morphology* – When predicting soft- and hard-
27 bodied prey specialization, the DAPC achieved 90.9% discrimination success, only marginally
28 confounding hard-bodied specialists with generalists (SM20). The main characters driving this
29 discrimination are involucrum length, heteroneme number, heteroneme volume, tentacle width,
30 total nematocyst volume, total haploneme volume, elastic strand width, and heteroneme
31 length. Discriminant analyses and GLM logistic regressions were also applied to specific
32 prey type presence and selectivity (Table 2 in the main text), revealing the sign of their
33 predictive relationship to each prey type. We only selected prey types with sufficient variation
34 in the data to carry out these analyses (copepods, fish, and large crustaceans). While the
35 presence of fish or large crustaceans in the diet cannot be unambiguously discriminated using
36 tentillum morphology (SM18,SM19), specialization on fish or large crustacean prey can be
37 fully disentangled (SM??). For each prey type studied, tentillum morphology is a much
38 better predictor of prey selectivity than of prey presence in the diet, despite prey selectivity
39 data being available for a smaller subset of species. Interestingly, many of the morphological
40 predictors had opposite slope signs when predicting prey selectivity *versus* predicting prey
41 presence in the diet (Table 2 in the main text).

42 *Evolution of tentillum and nematocyst characters* – One third of the characters measured
43 support a non-phylogenetic generative model, indicating they are not phylogenetically con-
44 served (SM13). Total nematocyst volume and cnidoband-to-heteroneme length ratio showed
45 strongly conserved phylogenetic signals. 74% of characters present a significant phylogenetic
46 signal, yet only total nematocyst volume, haploneme length, and heteroneme-to-cnidoband
47 length ratio had a phylogenetic signal with $K > 1$. 67% of characters support BM models,
48 indicating a history of neutral constant divergence. No relationship between phylogenetic
49 signal and BM model support was found. Haploneme nematocyst length is the only character
50 with support for an EB model of decreasing rate of evolution with time. No character had
51 support for a single-optimum OU model (when uninformed by feeding guild regime priors).

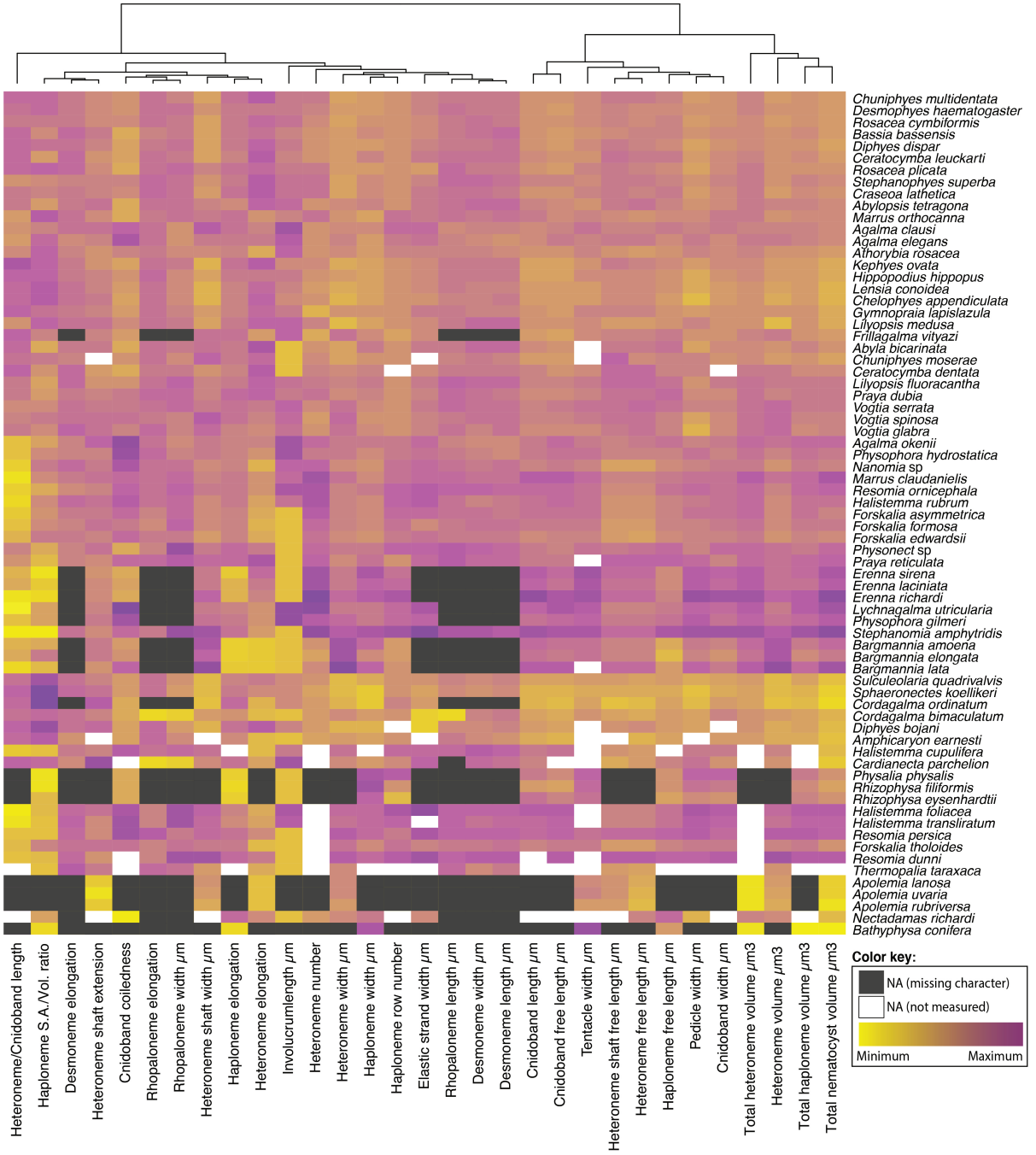


Figure 1: Heatmap summarizing the morphological diversity measured for 96 species of siphonophores clustered by similarity (raw data in Dryad repository). Missing values from absent characters presented as dark grey cells, missing values produced from technical difficulties presented as white cells. Values scaled by character.

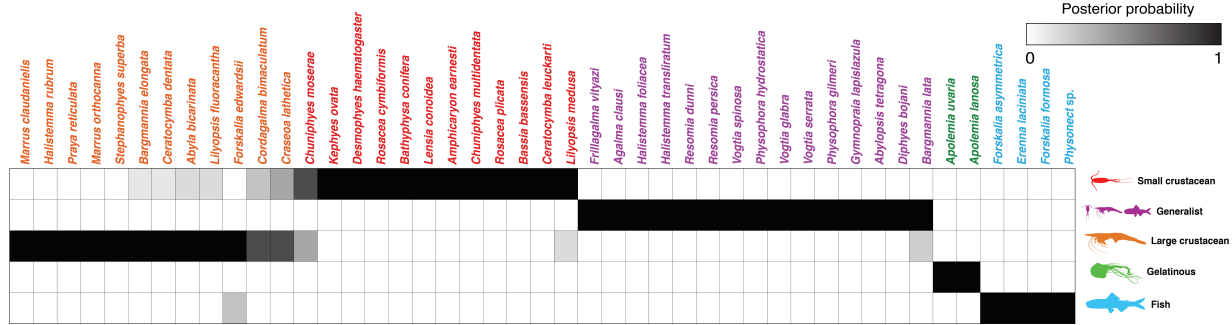


Figure 2: Hypothetical feeding guilds for siphonophore species predicted by a 6 PCA DAPC. Cell darkness indicates posterior probability of belonging to each guild. Training data set transformed so inapplicable states are computed as zeroes. Species ordered and colored according to their predicted feeding guild.

52 *Phenotypic integration of the tentillum* – Of the phylogenetic correlations (Fig. 3a, lower
 53 triangle), 81.3% were positive and 18.7% were negative, while of the ordinary correlations
 54 (Fig. 3a, upper triangle) 74.6% were positive and 25.4% were negative. Half (49.9%) of
 55 phylogenetic correlations were >0.5 , while only 3.6% are < -0.5 . Similarly, of the across-
 56 species correlations, 49.1% were >0.5 and only 1.5% were < -0.5 . We found that 13.9% of
 57 character pairs had opposing phylogenetic and ordinary correlation coefficients. Just 4% have
 58 negative phylogenetic and positive ordinary correlations (such as rhopaloneme elongation \sim
 59 heteroneme-to-cnidoband length ratio and haploneme elongation, or haploneme elongation \sim
 60 heteroneme number), and only 9.9% of character pairs had positive phylogenetic correlation
 61 yet negative ordinary correlation (such as heteroneme elongation \sim cnidoband convolution
 62 and involucrum length, or rhopaloneme elongation with cnidoband length). These disparities
 63 can be caused by Simpson's paradox (Blyth 1972): the reversal of the sign of a relationship
 64 when a third variable (or a phylogenetic topology (Uyeda et al. 2018)) is considered. However,
 65 no character pair had correlation coefficient differences larger than 0.64 between ordinary
 66 and phylogenetic correlations (heteroneme shaft extension \sim rhopaloneme elongation has a
 67 Pearson's correlation of 0.10 and a phylogenetic correlation of -0.54). Rhopaloneme elongation
 68 shows the most incongruencies between phylogenetic and ordinary correlations with other
 69 characters.

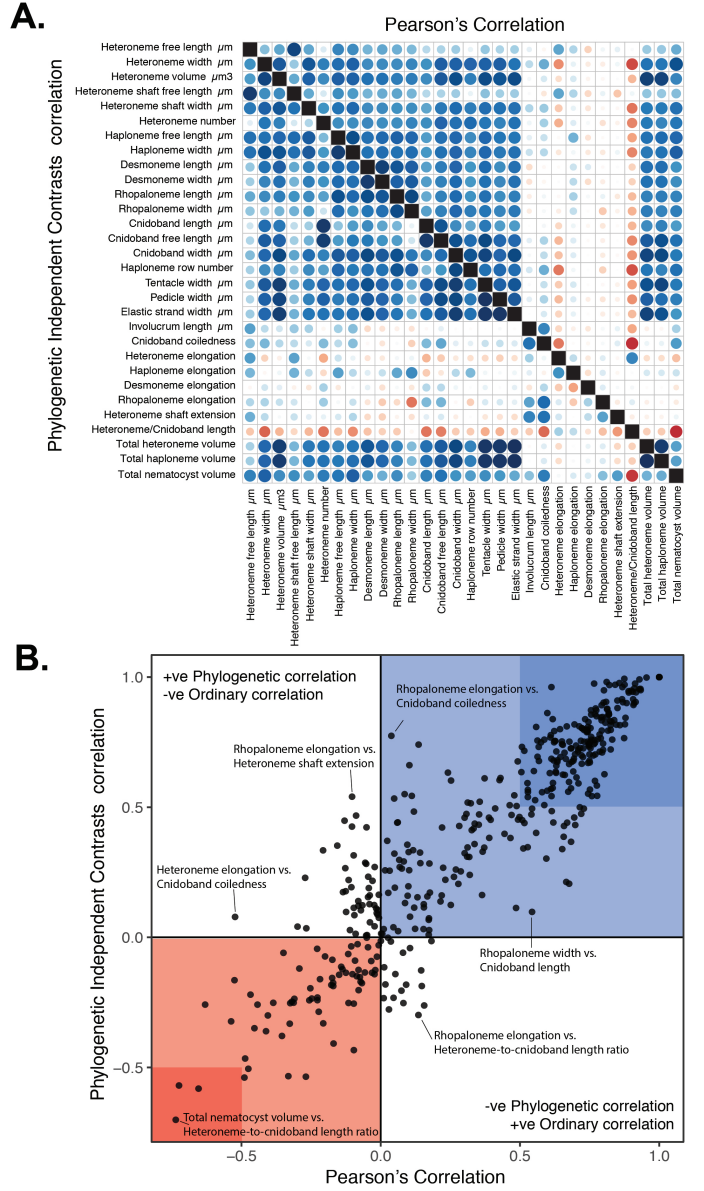


Figure 3: A. Correlogram showing strength of ordinary (upper triangle) and phylogenetic (lower triangle) correlations between characters. Both size and color of the circles indicate the strength of the correlation (R^2). B. Scatterplot of phylogenetic correlation against ordinary correlation showing a strong linear relationship ($R^2 = 0.92$, 95% confidence between 0.90 and 0.93). Light red and blue boxes indicate congruent negative and positive correlations respectively. Darker red and blue boxes indicate strong (<-0.5 or >0.5) negative and positive correlation coefficients respectively.

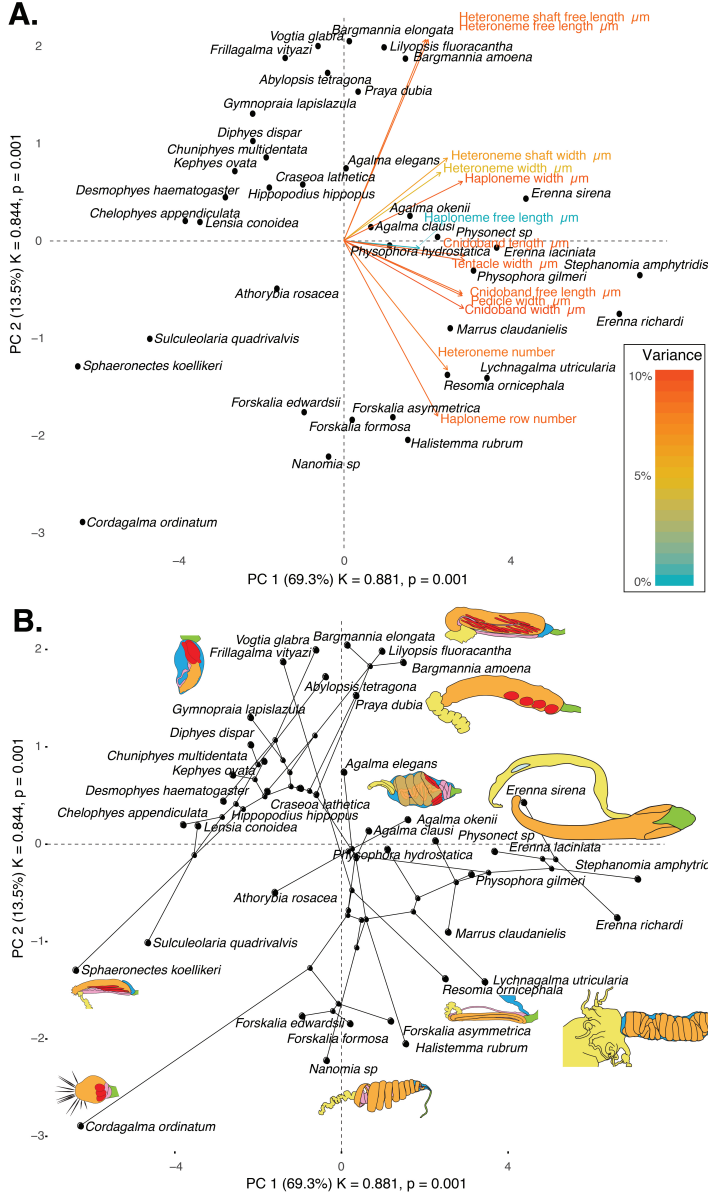


Figure 4: Phylomorphospace of the simple continuous characters principal components, excluding ratios and composite characters. A. Variance explained by each variable in the PC1-PC2 plane. Axis labels include the phylogenetic signal (K) for each component and p-value. B. Phylogenetic relationships between the species points distributed in that same space.

70 In the non-phylogenetic PCA morphospace using only simple characters (Fig. 4), PC1
71 (aligned with tentillum and tentacle size) explained 69.3% of the variation in the tentillum
72 morphospace, whereas PC2 (aligned with heteroneme length, heteroneme number, and
73 haploneme arrangement) explained 13.5%. In a phylogenetic PCA, 63% of the evolutionary
74 variation in the morphospace is explained by PC1 (aligned with shifts in tentillum size), while
75 18% is explained by PC2 (aligned with shifts in heteroneme number and involucrum length).

76 *Functional morphology of tentillum and nematocyst discharge* – Tentillum and nematocyst
77 discharge high speed measurements are available in Appendix 4. While the sample sizes of
78 these measurements were insufficient to draw reliable statistical results at a phylogenetic level,
79 we did observe patterns that may be relevant to their functional morphology. For example,
80 cnidoband length is strongly correlated with discharge speed (p value = 0.0002). This is
81 probably the sole driver of the considerable difference between euphysonect and calycophoran
82 tentilla discharge speeds (average discharge speeds: 225.0mm/s and 41.8mm/s respectively;
83 t-test p value = 0.011), since the euphysonects have larger tentilla than the calycophorans
84 among the species recorded.

85 We also observed that calycophoran haploneme tubules fire faster than those of eu-
86 physonects (T-test p value = 0.001). Haploneme nematocysts discharge 2.8x faster than
87 heteroneme nematocysts (T-test p value = 0.0012). Finally, we observed that the stenoteles
88 of the Euphysonectae discharge a helical filament that “drills” itself through the medium it
89 penetrates as it everts.

90 Supplementary Discussion

91 *Generating hypotheses on siphonophore feeding ecology* – One motivation for our research was
92 to understand the links between predator capture tools and their diets so we can generate
93 hypotheses about the diets of siphonophores based on morphological characteristics. Indeed,
94 our discriminant analyses were able to distinguish between different siphonophore diets
95 based on morphological characters alone. The models produced by these analyses generated

96 testable predictions about the diets of many species for which we only have morphological
97 data of their tentacles. While the limited dataset used here is informative for generating
98 tentative hypotheses, the empirical dietary data are still scarce and insufficient to cast robust
99 predictions. This reveals the need to extensively characterize siphonophore diets and feeding
100 habits. In future work, we can test these ecological hypotheses and validate these models
101 by directly characterizing the diets of some of those siphonophore species. Predicting diet
102 using morphology is a powerful tool to reconstruct food web topologies from community
103 composition alone. In many of the ecological models found in the literature, interactions
104 among the oceanic zooplankton have been treated as a black box (Mitra 2009). The ability
105 to predict such interactions, including those of siphonophores and their prey, will enhance
106 the taxonomic resolution of nutrient-flow models constructed from plankton community
107 composition data.

108 *Evolutionary history of tentillum morphology* –This study produced the most speciose
109 siphonophore molecular phylogeny to date, while incorporating the most recent findings
110 in siphonophore deep node relationships. This phylogeny revealed for the first time that
111 the genus *Erenna* is the sister to *Stephanomia amphytridis*. *Erenna* and *Stephanomia* bear
112 the largest tentilla among all siphonophores, thus their monophyly indicates that there was
113 a single evolutionary transition to giant tentilla. Siphonophore tentilla range in size from
114 ~30 µm in some *Cordagalma* specimens to 2-4 cm in *Erenna* species, and up to 8 cm in
115 *Stephanomia amphytridis* (Pugh and Baxter 2014). Most siphonophore tentilla measure
116 between 175 and 1007 µm (1st and 3rd quartiles), with a median of 373 µm. The extreme
117 gain of tentillum size in this newly found clade may have important implications for access
118 to large prey size classes.

119 Siphonophore tentilla are defined as lateral, monostichous evaginations of the tentacle
120 gastrovascular lumen with epidermal nematocysts (Totton and Bargmann 1965). The buttons
121 on *Physalia* tentacles were not traditionally regarded as tentilla, but (Bardi and Marques
122 2007) and our observations (Munro et al. 2018), confirm that the buttons contain evaginations

¹²³ of the gastrovascular lumen, thus satisfying all the criteria for the definition. In this light,
¹²⁴ and given that most Cystonectae bear conspicuous tentilla, we conclude (in agreement with
¹²⁵ (Munro et al. 2018)) that tentilla are likely ancestral to all siphonophores, and secondarily
¹²⁶ lost in *Apolemia* and *Bathyphysa conifera*.

¹²⁷ The clade Tendiculophora contains far more species than its relatives Cystonectae, Apolemi-
¹²⁸ idae, and Pyrostephidae. An increase in clade richness and ecological diversification can
¹²⁹ be triggered by a ‘key innovation’ (Simpson 1955). The evolutionary innovation of the
¹³⁰ Tendiculophora tentilla with shooting cnidobands and modular regions may have facilitated
¹³¹ further dietary diversification.

2.1) Definitions of homologous structures used throughout this work.

Structure	Definition
Haploneme	Nematocyst with no shaft
Heteroneme	Nematocyst with a distinct shaft
Desmoneme	Small oval/tapered adhesive nematocyst with thick coiled tubule
Rhopaloneme	Small rod-like nematocyst found on the terminal filament
Terminal filament	Distal extension of the tentillum beyond the cnidoband
Cnidoband	Distinct packing of nematocysts on the dorsal side of the tentillum
Tentacle	Tubular projection from the gastrozooid basigaster
Tentillum	Evenly spaced dorsal evagination of the tentacle carrying ordered and functional nematocysts
Involutrum	Extension of the pedicle covering part of the cnidoband
Pedicle	Proximal region of the tentillum between the cnidoband and the tentacle
Elastic strand	Mesoglea derived collagenous double strand underlying the cnidoband of some siphonophores

2.2) Definitions of the continuous morphological and kinematic characters measured.

Character	Definition	Units
Cnidoband length	Distance from the base to the tip of the cnidoband in natural position	micrometers
Cnidoband free length	Distance from the base to the tip of the cnidoband when stretched straight	micrometers
Cnidoband width	Diameter of the cnidoband on the widest point	micrometers
Involutrum length	Length of the involutrum from the base of the cnidoband to its most distal extent	micrometers
Heteroneme length	Length of the heteronomes	micrometers
Heteroneme width	Diameter of the heteronomes at the widest point	micrometers
Heteroneme shaft length	Length of the heteroneme shaft	micrometers
Heteroneme shaft width	Width of the heteroneme shaft	micrometers
Heteroneme number	Number of heteronomes in each tentillum (# in each row*2)	micrometers
Haploneme length	Length of the haplonemes	micrometers
Haploneme width	Diameter of the haplonemes at the widest point	micrometers
Rhopaloneme length	Length of the rhopalonemes	micrometers
Rhopaloneme width	Diameter of the rhopalonemes at the widest point	micrometers
Desmoneme length	Length of the desmonemes	micrometers
Desmoneme width	Diameter of the cnidoband at the widest point	micrometers
Involutrum length	Length of the involutrum from the base of the cnidoband to its most distal extent	micrometers
Elastic strand width	Diameter of the descending elastic strand at the widest point	micrometers
Pedicle width	Diameter of the pedicle	micrometers
Tentacle width	Diameter of the tentacle	micrometers
Haploneme row number	Number of haploneme rows running parallel to the length of the cnidoband	micrometers
Cnidoband coiledness	Cnidoband free length / Cnidoband length	adimensional
Heteroneme elongation	Heteroneme Length/Width	adimensional
Haploneme elongation	Haploneme Length/Width	adimensional
Desmoneme elongation	Desmoneme Length/Width	adimensional
Rhopaloneme elongation	Rhopaloneme Length/Width	adimensional
Heteroneme shaft extension	Heteroneme shaft length / Heteroneme capsule length	adimensional
Nematocyst Surface area	$4\pi * 2^2 * ((Length/2)^1.6) * ((Width/2)^2 * 1.6) / 3 * 1/1.6$	micrometers squared
Nematocyst volume	Ellipsoid formula : $(4/3)\pi * (Length/2) * (Width/2)^2$	micrometers cubed
Nematocyst S/V ratio	Nematocyst surface area / Nematocyst volume	1/micrometers
Total haploneme volume	Haploneme volume * Haploneme row number * (Cnidoband free length / Haploneme width)	micrometers cubed
Total heteroneme volume	Heteroneme volume * Heteroneme number	micrometers cubed
Total nematocyst volume	Total haploneme volume + Total heteroneme volume	micrometers cubed
Total discharge time	Time from initial cnidoband movement to complete conformational change	milliseconds
Average CB discharge speed	Distance covered by the leading edge of the discharging cnidoband in the total discharge time.	mm/s
Maximum CB discharge speed	Maximum speed attained by the leading edge of the discharging cnidoband	mm/s
Heteroneme discharge speed AVG	Distance covered by the heteroneme nematocyst tubule from initial ejection to full eversion in the time it takes to evert fully.	mm/s
Heteroneme discharge free speed AVG	Distance covered by the heteroneme nematocyst tubule in the time it takes to evert fully, accounting for coiling.	mm/s
Heteroneme discharge speed MAX	Maximum speed attained by the non-shaft tube of the heteroneme nematocysts during eversion.	mm/s
Heteroneme discharge free speed MAX	Maximum speed attained by the non-shaft tube of the heteroneme nematocysts during eversion, accounting for coiling.	mm/s
Heteroneme shaft discharge speed MAX	Maximum speed attained by the shaft of the tubule of the heteroneme nematocysts during initial eversion.	mm/s
Heteroneme filament length	Distance covered by the heteroneme nematocyst tubule from initial ejection to full eversion	micrometers
Haploneme discharge speed AVG	Distance covered by the haploneme nematocyst tubule from initial ejection to full eversion in the time it takes to evert fully.	mm/s

Figure 5: Character definitions.

132 Supplementary Materials

133 Other trees inferred in this work include:

134 The constrained tree inferences utilized the following constrain topology:



Figure 6: Maximum likelihood IQTree inference, unconstrained. Node labels are bootstrap support values.

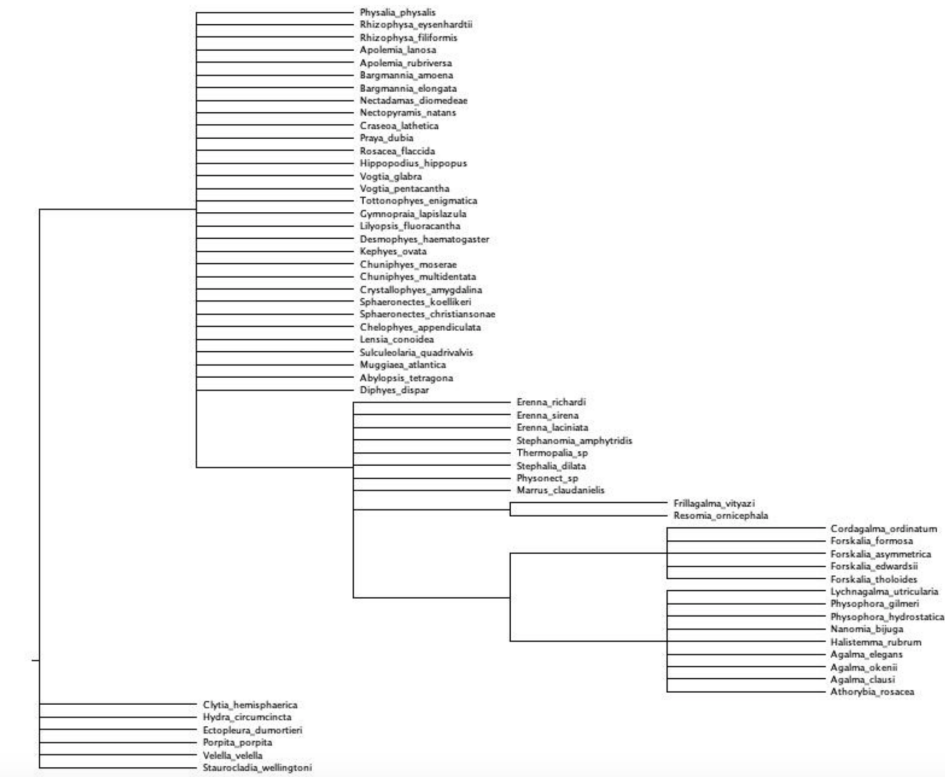


Figure 7: Topology used to constrain analyses (minimal topological statements based on the incongruences between the unconstrained tree and Munro et al. (2018)).

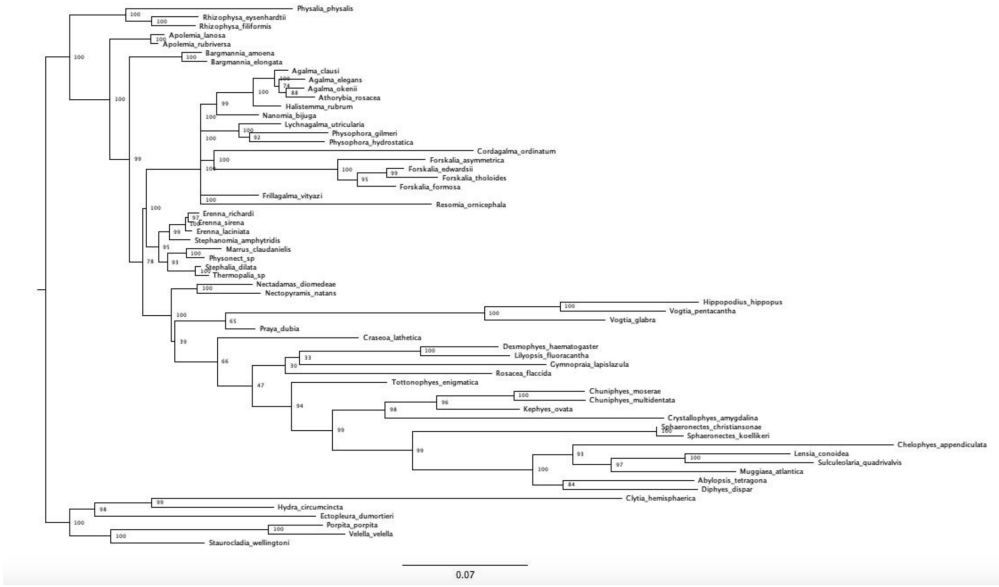


Figure 8: Constrained IQTree ML inference. Node labels are bootstrap support values.

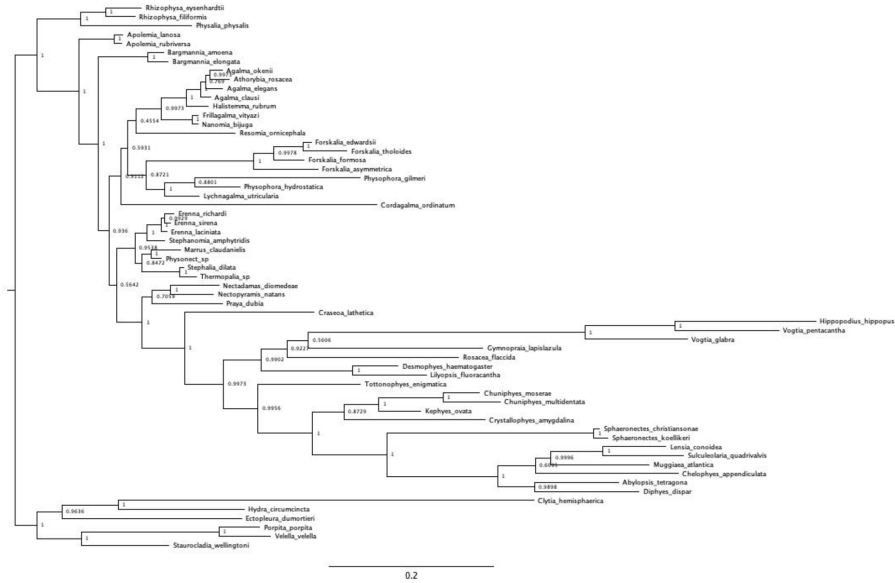


Figure 9: Unconstrained Bayesian topology inference in RevBayes (node labels are Bayesian posteriors).



Figure 10: Clade constrained Bayesian inference in RevBayes (node labels are Bayesian posteriors).

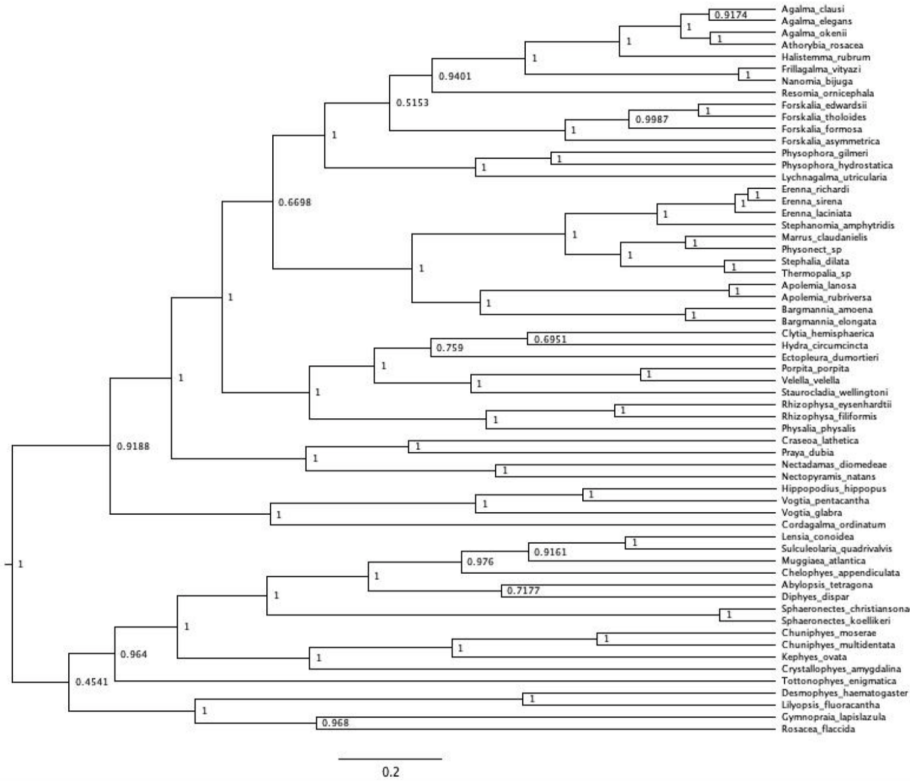


Figure 11: Unconstrained ultrametric Bayesian time tree branch length and topology inference in RevBayes (node labels are Bayesian posteriors). Arbitrary rooting.).

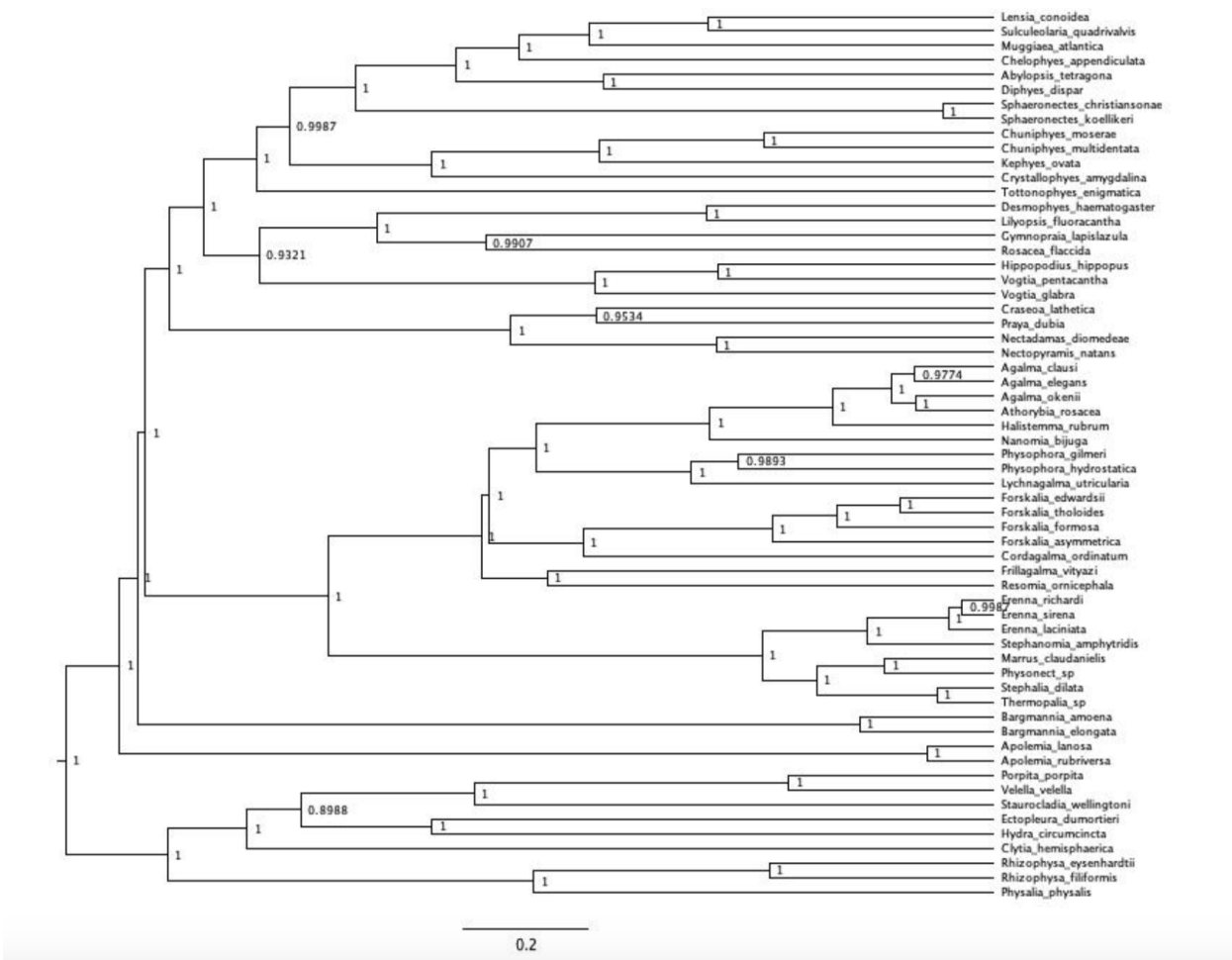


Figure 12: Ultrametric Bayesian time tree branch length inference in RevBayes (node labels are bayesian posteriors). Topology clamped to the Bayesian constrained topology inference in @ref{Bayes_constrained}. Tree rooted using outgroup constraint.

Character	Non-Phylogenetic dAIC	BM dAIC	EB dAIC	OU dAIC	K	K p-value	Ntaxa
Haploneme elongation	0	2.017	4.332	2.38	0.583	0.001	43
Desmoneme elongation	0	3.232	5.693	3.183	0.018	0.864	31
Heteroneme shaft width μm	0	5.346	7.67	2.581	0.45	0.005	42
Elastic strand width μm	0	1526	3.938	1.296	0.706	0.001	34
Desmoneme length μm	0.518	0	2.46	0.578	0.566	0.002	31
Heteroneme shaft extension	0.589	0	2.324	1.965	0.041	0.970	42
Haploneme SA/V	0.91	0	2.315	2.291	0.156	0.132	43
Total heteroneme volume μm^3	0.961	0	2.352	2.328	0.248	0.046	39
Rhopaloneme width μm	1.205	0	2.46	1.321	0.308	0.123	31
Heteroneme volume μm^3	2.002	0	2.153	2.324	0.196	0.117	42
Involucrum length μm	2.479	0	2.498	2.492	0.529	0.001	29
Tentacle width μm	2.939	0	2.307	1.974	0.367	0.044	44
Cnidoband coiledness	3.077	0	2.315	1.786	0.174	0.043	43
Total haploneme volume μm^3	3.641	0	1.852	2.296	0.198	0.267	43
Cnidoband free length μm	3.801	0	2.132	2.315	0.325	0.007	43
Heteroneme free length μm	3.82	0	2.01	1.325	0.301	0.080	42
Rhopaloneme elongation	3.852	0	2.145	2.46	0.062	0.827	31
Desmoneme width μm	3.96	0	2.46	2.121	0.553	0.004	31
Cnidoband length μm	4.094	0	1.911	2.315	0.321	0.015	43
Heteroneme number	4.262	0	2.352	2.219	0.866	0.001	39
Heteroneme shaft free length μm	4.553	0	2.324	2.321	0.331	0.126	42
Rhopaloneme length μm	5.599	0	2.46	2.457	0.589	0.001	31
Heteroneme/Cnidoband length	5.671	0	1.862	2.342	1.068	0.001	42
Pedicle width μm	6.566	0	2.253	2.315	0.541	0.001	43
Haploneme width μm	7.495	0	2.218	2.304	0.553	0.001	43
Heteroneme width μm	7.53	0	2.324	1.647	0.502	0.001	42
Heteroneme elongation	14.169	0	0.819	2.23	0.508	0.001	42
Haploneme row number	19.566	0	2.114	2.315	0.442	0.001	43
Total nematocyst volume μm^3	21.007	0	2.213	2.292	1.3	0.001	45
Cnidoband width μm	5.69	0.307	0	2.623	0.374	0.001	43
Haploneme free length μm	12.337	7.125	0	9.439	1.079	0.001	43

Non-phylogenetic model supported

Brownian Motion model supported

Early Burst model supported

Figure 13: Model support (delta AICc), phylogenetic signal (Blomberg's K), and phylogenetic signal permutation test p-value for each continuous character. Ntaxa = Number of taxa used in the analyses after removing those where the character state is inapplicable or the data is missing.

Variable	Best model	Msig	Cvar	Svar	Sasr	Shgt	Dcfid
Desmoneme length μm	WN	0.889	0.224	0.084	0.32	0.146	0
Heteroneme shaft extension	WN	0.861	0	0.577	0	0.533	0.042
Total heteroneme volume	WN	0.895	0.577	0.006	0.026	0.078	0.603
Rhopaloneme width μm	WN	0.823	0.42	0.182	0.014	0.531	0.006
Haploneme free length μm	EB	0.841	0.052	0.036	0.168	0.226	0.843
Heteroneme volume μm^3	BM	0.855	0.731	0.228	0.897	0.775	0.104
Involucrum length μm	BM	0.839	0.01	0.018	0.116	0.09	0.987
Tentacle width μm	BM	0.817	0.841	0.402	0.386	0.785	0.48
Cnidoband coiledness	BM	0.873	0	0.028	0.016	0.144	0.41
Total haploneme volume	BM	0.807	0.228	0.004	0.006	0.024	0.398
Cnidoband free length μm	BM	0.825	0.076	0.002	0	0.006	0.681
Heteroneme free length μm	BM	0.859	0.392	0.386	0.056	0.591	0.284
Rhopaloneme elongation	BM	0.873	0.022	0.006	0.004	0.048	0.104
Desmoneme width μm	BM	0.813	0.877	0.531	0.014	0.941	0.014
Cnidoband length μm	BM	0.829	0.096	0	0	0.004	0.901
Heteroneme number	BM	0.823	0.312	0	0.004	0.02	0.869
Heteroneme shaft free length μm	BM	0.877	0.468	0.565	0.034	0.841	0.851
Rhopaloneme length μm	BM	0.829	0.525	0.547	0.01	0.917	0.08
Heteroneme/cnidoband length	BM	0.839	0.01	0	0.004	0.008	0.715
Cnidoband width μm	BM	0.907	0.977	0	0.002	0.01	0.11
Pedicle width μm	BM	0.817	0.931	0.476	0.088	0.969	0.813
Haploneme width μm	BM	0.881	0.805	0.12	0.294	0.511	0.15
Heteroneme width μm	BM	0.849	0.142	0.156	0.356	0.819	0.278
Heteroneme elongation	BM	0.933	0.094	0.07	0.681	0.791	0.777
Haploneme row number	BM	0.863	0	0.002	0.004	0.008	0.012

Figure 14: Model adequacy scores for the best model supported for each morphological character. Cvar = coefficient of variation of the absolute value of the contrasts. Svar = Slope of a linear model fitted to the absolute value of the contrasts against their expected variances. Sasr = slope of the contrasts against the ancestral state inferred at each corresponding node. Shgt = slope of the contrasts against node depth. Dcfid = Kolmogorov-Smirnov D-statistic comparing contrasts to a normal distribution with SD equal to the root of the mean of squared contrasts.

Character	N	dAICc BM	dAICc OU1	dAICc OUm	Msig	Cvar	Svar	Sasr	Shgt	Dcfid	
Haploneme elongation	21	0	0.953	713.671	0.801	0	0.038	0.156	0.362	0.098	
Heteroneme shaft width μm	19	0	1.051	632.503	0.767	0.801	0.128	0.092	0.4	0.813	
Cnidoband width μm	21	0	1.595	761.241	0.781	0.723	0.072	0.09	0.31	0.228	
Heteroneme shaft free length μm	19	0	1.649	628.334	0.791	0.402	0.941	0.098	0.575	0.464	
Heteroneme volume μm^3	19	0	2.105	629.21	0.779	0.034	0.39	0.338	0.637	0.392	
Haploneme width μm	21	0	2.452	766.546	0.779	0.599	0.316	0.791	0.995	0.288	
Pedicle width μm	21	0	2.458	764.406	0.815	0.791	0.368	0.26	0.963	0.298	
Heteroneme width μm	19	0	2.516	634.229	0.805	0.809	0.292	0.208	0.709	0.38	
Tentacle width μm	22	0	2.702	383.12	0.835	0.496	0.344	0.867	0.096	0.444	
Heteroneme to CB	19	0	0.127	NA		0.811	0.336	0.004	0.068	0.026	0.434
Haploneme surface area:volume	21	0	2.282	757.267	0.747	0.563	0.392	0.583	0.927	0.15	
Heteroneme elongation	19	0.217	0	618.621	0.819	0.601	0.012	0.707	0.062	0.715	
Total nematocyst volume	22	0.57	0	378.872	0.809	0.501	0.06	0.088	0.266	0.501	
Heteroneme free length μm	19	0.746	0	627.372	0.811	0.885	0.593	0.156	0.368	0.679	
Total haploneme volume	21	1.281	0	730.592	0.829	0.452	0.038	0.134	0.096	0.819	
Cnidoband length μm	21	1.439	0	763.478	0.761	0.328	0.04	0.11	0.098	0.803	
Cnidoband free length μm	21	2.219	0	760.518	0.843	0.35	0.012	0.066	0.05	0.911	
Cnidoband coiledness	21	2.669	0	765.921	0.807	0.002	0.008	0.03	0.076	0.791	
Haploneme row number	21	4.177	0	729.95	0.825	0.004	0.002	0.06	0.006	0.346	
Haploneme free length μm	21	5.497	0	778.011	0.793	0.388	0.032	0	0.052	0.306	
Heteroneme shaft extension	19	6.17	0	611.533	0.775	0	0.068	0.665	0.124	0.184	
Rhopaloneme elongation	13	144.229	146.783	0	0.753	0.641	0.434	0.188	0.933	0.617	
Desmoneme length μm	13	148.14	151.403	0	0.763	0.182	0.607	0.31	0.745	0.014	
Rhopaloneme length μm	13	150.731	154.198	0	0.739	0.803	0.24	0.03	0.14	0.316	
Rhopaloneme width μm	13	150.82	154.287	0	0.743	0.462	0.306	0.07	0.182	0.092	
Desmoneme elongation	13	159.594	158.584	0	0.719	0.206	0.074	0.094	0.036	0.993	
Desmoneme width μm	13	164.639	168.106	0	0.773	0.11	0.885	0.098	0.605	0.002	
Involucrum length μm	14	148.672	151.078	0	0.779	0.126	0.17	0.25	0.418	0.671	
Elastic strand width μm	15	473.984	477.156	0	0.827	0.921	0.184	0.064	0.953	0.785	
Total heteroneme volume	17	619.03	619.932	0	0.797	0.803	0.078	0.172	0.35	0.697	
Heteroneme number	17	620.836	620.193	0	0.777	0.39	0.008	0.074	0.056	0.054	

Brownian Motion Supported

Single Optimum OU Supported

Multiple Optima OU Supported

Figure 15: Model support (delta AICc) for each morphological character analyzed on the feeding guild reconstruction regime tree. OU1 = Single-optimum Ornstein-Uhlenbeck. OUm = Multi-optima Ornstein-Uhlenbeck. Model adequacy scores calculated for the best supported model only. Msig = mean of squared contrasts. Cvar = coefficient of variation of the absolute value of the contrasts. Svar = Slope of a linear model fitted to the absolute value of the contrasts against their expected variances. Sasr = slope of the contrasts against the ancestral state inferred at each corresponding node. Shgt = slope of the contrasts against node depth. Dcfid = Kolmogorov-Smirnov D-statistic comparing contrasts to a normal distribution with SD equal to the root of the mean of squared contrasts.

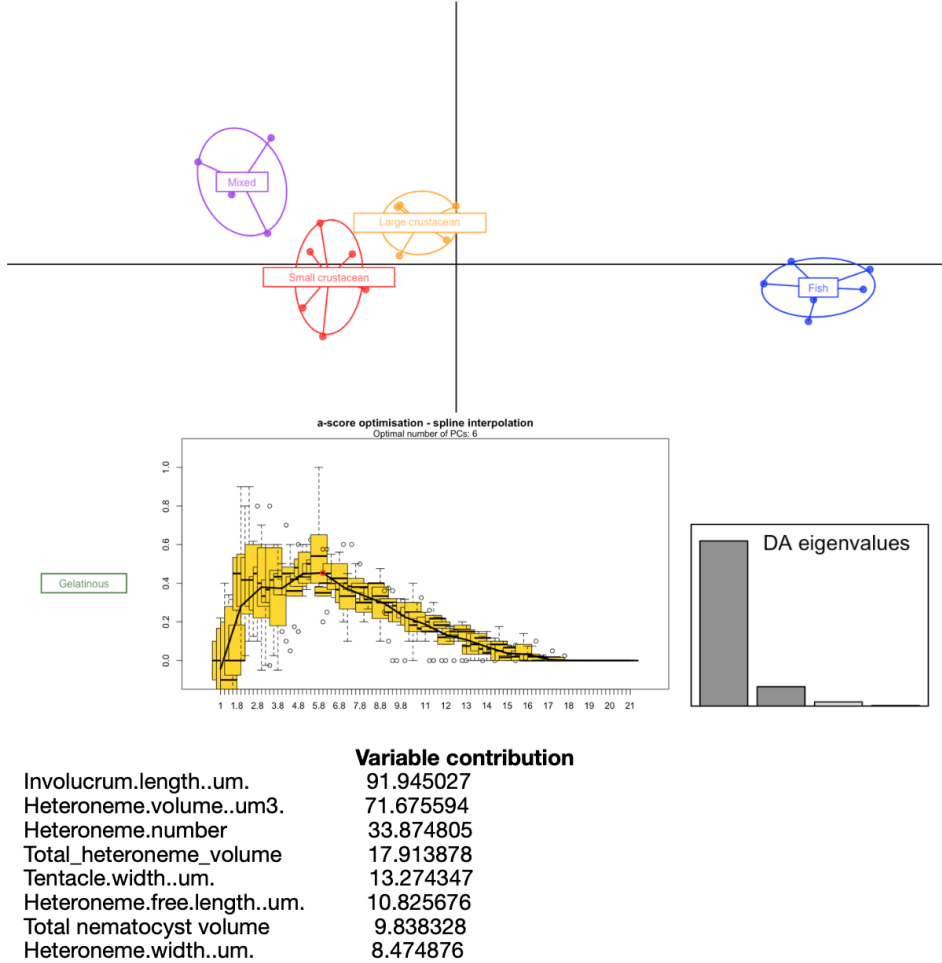
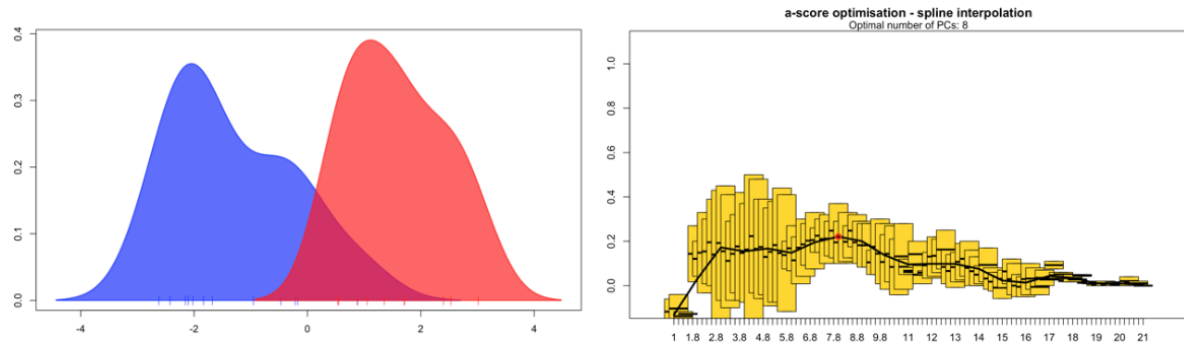


Figure 16: DAPC for Feeding guilds. Six PCs retained after a-score optimization (100 iterations). Four LDA functions used. Discriminant power on training set: 100%. Prediction posterior distribution heat map in main text Figure 6. Variable contribution (top quartile) calculated by the sum of the LDA variable loadings weighted by the eigenvalue of each LDA.



Variable contribution

Total_nematocyst_volume	12.810953
Tentacle.width..um.	5.687086
haploneme_elongation	4.586386
SAV_haploneme	4.264843
Haploneme.row.number..um.	2.966009
Cnidoband.length..um.	1.959479
Cnidoband.width..um.	1.679753
Cnidoband.free.length..um.	1.468262

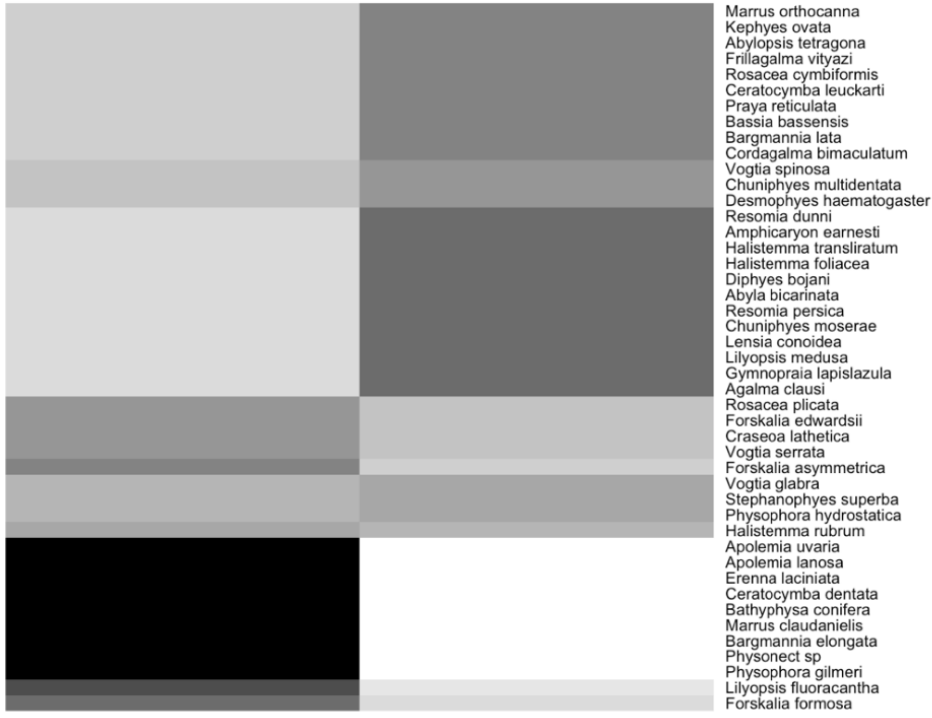
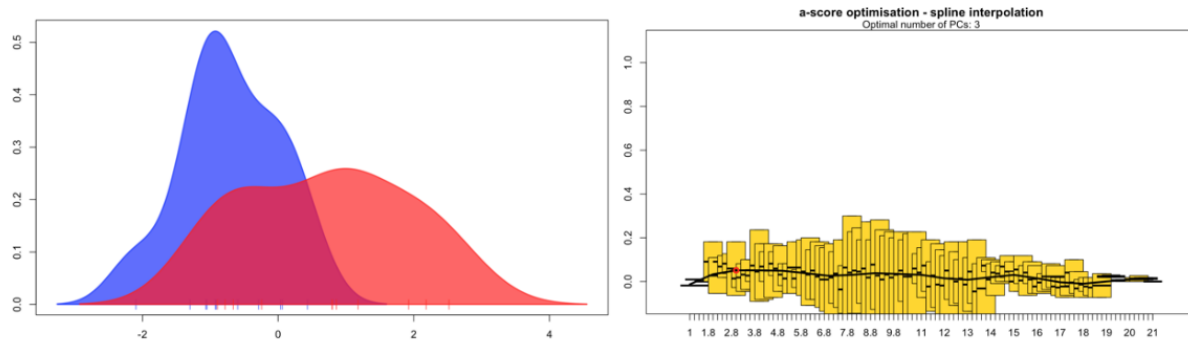


Figure 17: DAPC for copepod presence in the diet. Eight PCs retained after a-score optimization (100 iterations). One LDA functions used. Discriminant power on training set: 95.4%. Grayscale heat map shows the posterior probability distribution of the predictions. Variable contribution (top quartile) calculated by the sum of the LDA variable loadings weighted by the eigenvalue of each LDA.



Variable contribution

total_haploneme_volume	2.2734508
Heteroneme.volume..um3.	1.1308252
total_nematocyst_volume	1.1104459
total_heteroneme_volume	0.9402038
Cnidoband.length..um.	0.7583124
Cnidoband.free.length..um.	0.6650068
Involucrum.length..um.	0.6097537
Pedicle.width..um.	0.5447312

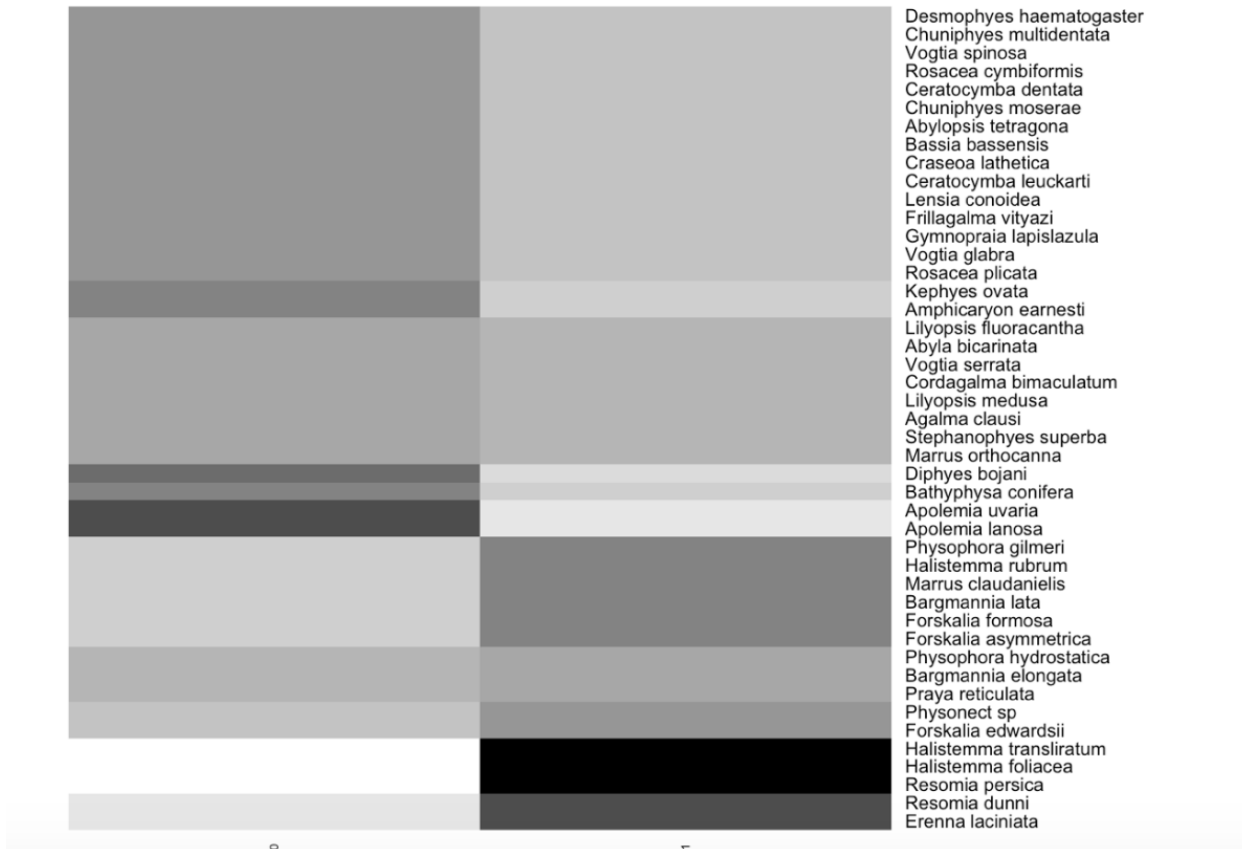
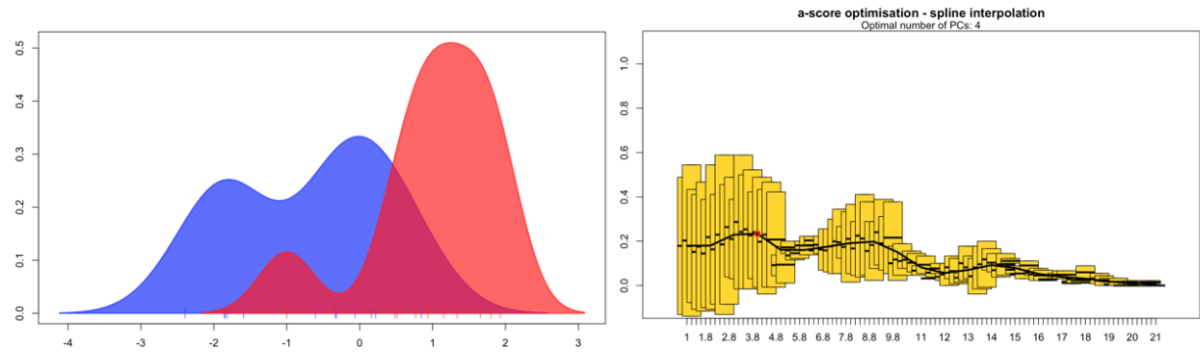


Figure 18: DAPC for fish presence in the diet. Three PCs retained after a-score optimization (100 iterations). One LDA function used. Discriminant power on training set: 68.1%. Grayscale heat map shows the posterior probability distribution of the predictions. Variable contribution (top quartile) calculated by the sum of the LDA variable loadings weighted by the eigenvalue of each LDA.



Variable contribution

	Variable contribution
Involucrum.length..um.	8.4739326
total_heteroneme_volume	2.0479062
Elastic.strand.width..um.	1.2640038
Rhopaloneme.length..um.	0.4274179
Heteroneme.volume..um3	0.4255758
haploneme_elongation	0.3530771
Desmoneme.length..um.	0.3274451
Tentacle.width..um.	0.2763979

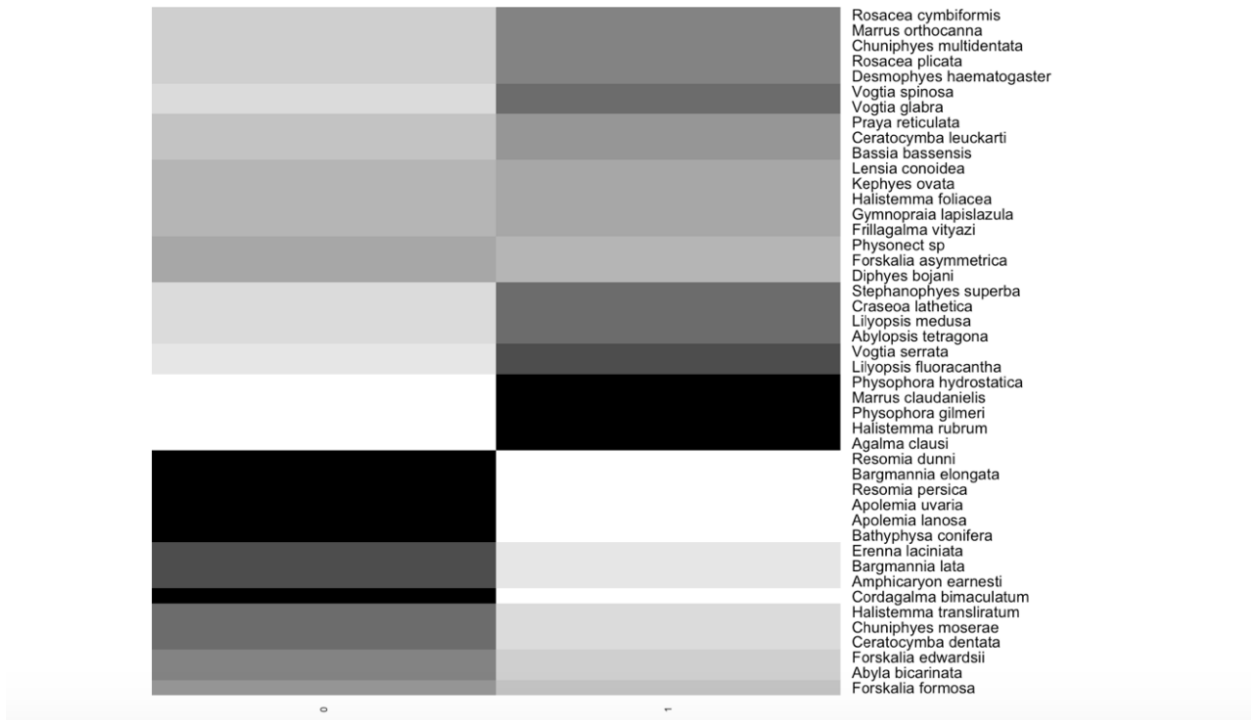
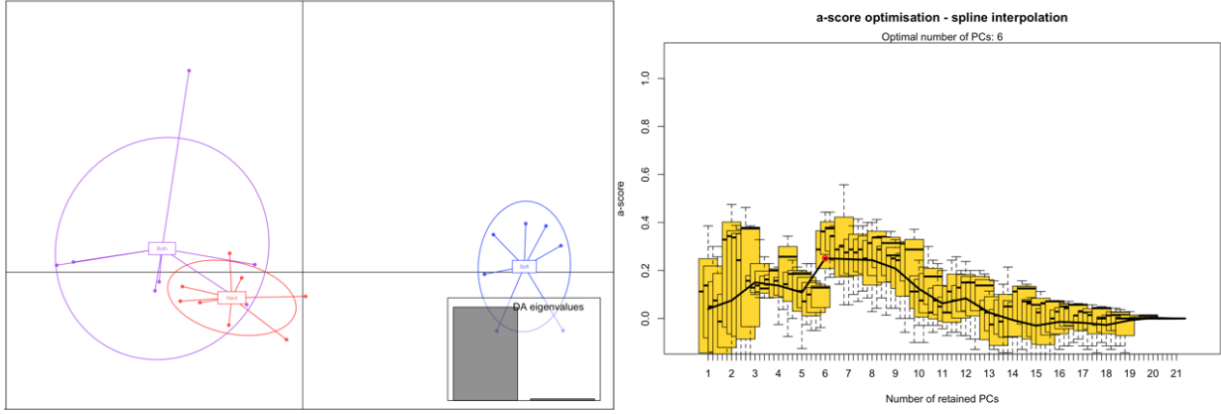


Figure 19: DAPC for large crustacean presence in the diet. Four PCs retained after a-score optimization (100 iterations). One LDA function used. Discriminant power on training set: 81.8%. Grayscale heat map shows the posterior probability distribution of the predictions. Variable contribution (top quartile) calculated by the sum of the LDA variable loadings weighted by the eigenvalue of each LDA.



Variable contribution

Involucrum.length..um.	24.425696
Heteroneme.number	18.129947
Heteroneme.volume..um3.	6.849738
Tentacle.width..um.	6.587487
Total_nematocyst_volume	5.606488
total_haploneme_volume	4.185115
Elastic.strand.width..um.	3.584917
Heteroneme.free.length..um.	3.014292

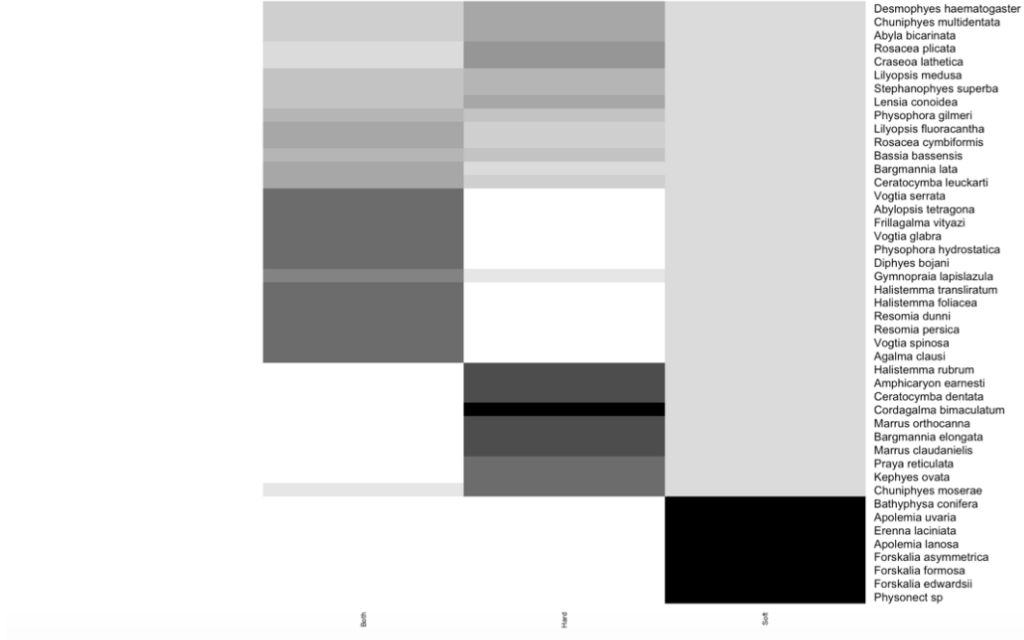


Figure 20: DAPC for soft-bodied vs. hard bodied prey specialization. Six PCs retained after a-score optimization (100 iterations). Two LDA functions used. Discriminant power on training set: 90.9%. Grayscale heat map shows the posterior probability distribution of the predictions. Variable contribution (top quartile) calculated by the sum of the LDA variable loadings weighted by the eigenvalue of each LDA.

Character	Prey type	Ntaxa	phyloGLM AIC	phyloGLM P	phyloglm b	GLM AIC	GLM P	GLM b
Cnidoband coiledness	Decapod diet	21	23.701	0.029	2.327	21.762	0.016	3.227
Haploneme surface area:volume	Copepod diet	21	19.143	0.017	3.246	17.355	0.017	4.631
Haploneme width μm	Copepod diet	21	18.844	0.017	-3.098	16.997	0.019	-4.417
Pedicle width μm	Copepod diet	21	22.182	0.032	-1.16	23.723	0.024	-1.437
Tentacle width μm	Copepod diet	22	22.038	0.026	-1.543	23.634	0.025	-1.505
Cnidoband length μm	Copepod diet	21	23.431	0.042	-0.864	24.178	0.025	-1.131
Cnidoband width μm	Copepod diet	21	22.887	0.035	-1.545	23.658	0.027	-1.89
Heteroneme number	Copepod diet	17	20.52	0.059	-0.718	19.615	0.03	-0.973
Total haploneme volume	Copepod diet	21	23.507	0.03	-0.581	25.232	0.031	-0.578
Total heteroneme volume	Copepod diet	17	17.156	0.032	-0.533	16.369	0.031	-0.758
Pedicle width μm	Ostracod diet	21	17.523	0.041	-1.43	15.165	0.035	-1.97
Heteroneme shaft free length μm	Copepod diet	19	23.955	0.076	-1.53	23.378	0.04	-2.16
Haploneme width μm	Fish diet	21	28.118	0.091	1.268	27.551	0.043	1.642
Tentacle width μm	Fish diet	22	28.927	0.058	0.804	28.771	0.044	0.874
Haploneme surface area:volume	Fish diet	21	28.258	0.098	-1.329	27.596	0.044	-1.768
Total haploneme volume	Ostracod diet	21	20.028	0.043	-0.619	17.733	0.046	-0.681
Heteroneme volume μm^3	Copepod diet	19	24.282	0.091	-0.521	24.297	0.046	-0.72
Pedicle width μm	Fish diet	21	28.21	0.074	0.815	27.839	0.049	0.918

Figure 21: Logistic regressions between continuous morphological characters and prey type presences. Ntaxa = number of taxa used in the analyses after removing taxa with missing diet data and inapplicable character states. phyloGLM = Phylogenetic generalized logistic regression model. GLM = Generalized logistic regression model. P = p-value. b = slope. Only cases with significant GLM fits were retained. Cells colored blue indicate phyloGLM p-value < 0.05. Cells colored green indicate GLM p-value < 0.05

136 Ordinary and phylogenetic logistic regression of morphological characters and the pres-

137 ence/absence of prey types:

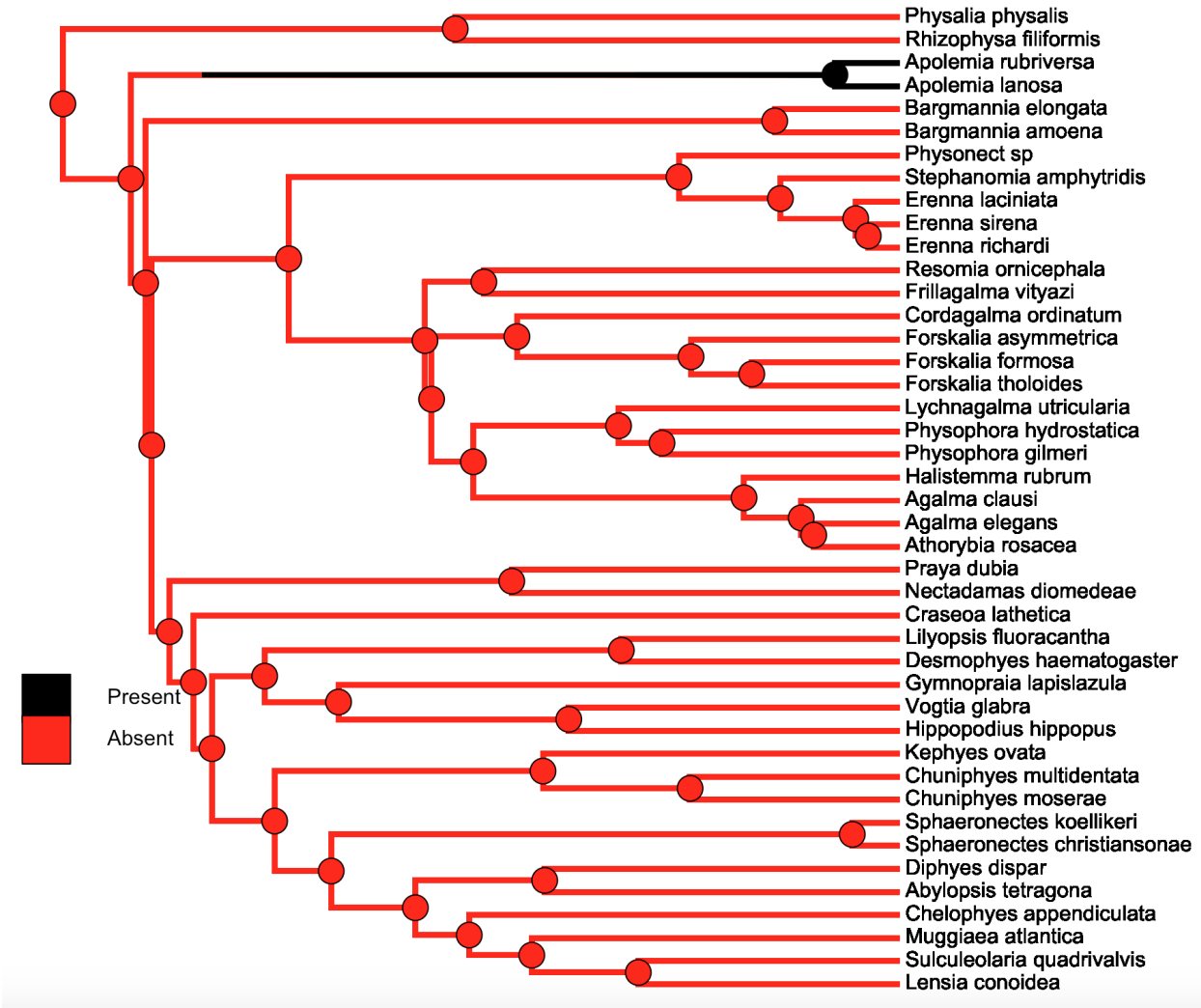


Figure 22: SIMMAP Tentilla presence/absence.

138

SIMMAP ancestral reconstructions of categorical characters:



Figure 23: SIMMAP Cnidoband proximal heteroneme presence/absence.

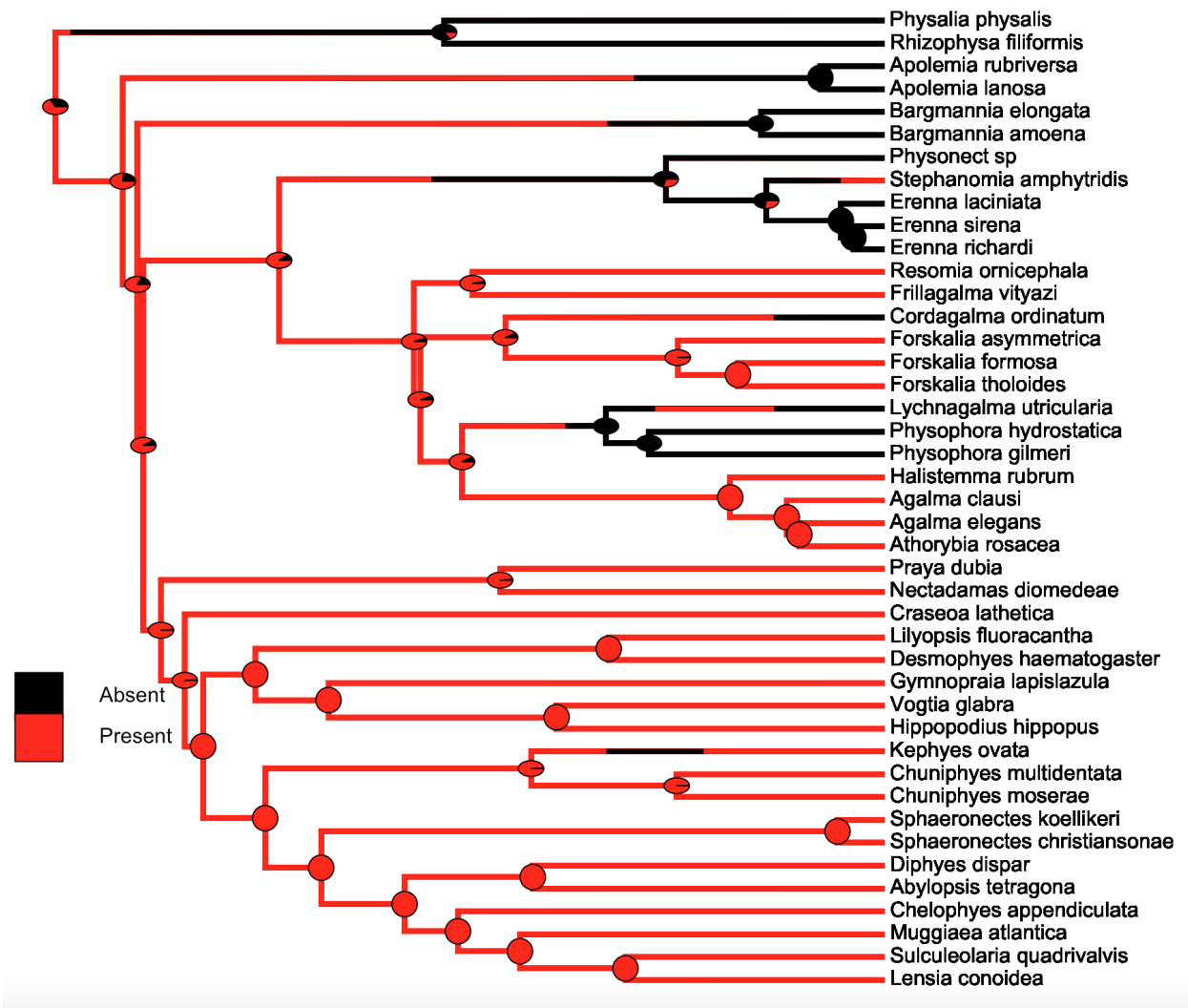


Figure 24: SIMMAP Desmoneme+Rhopaloneme presence/absence.

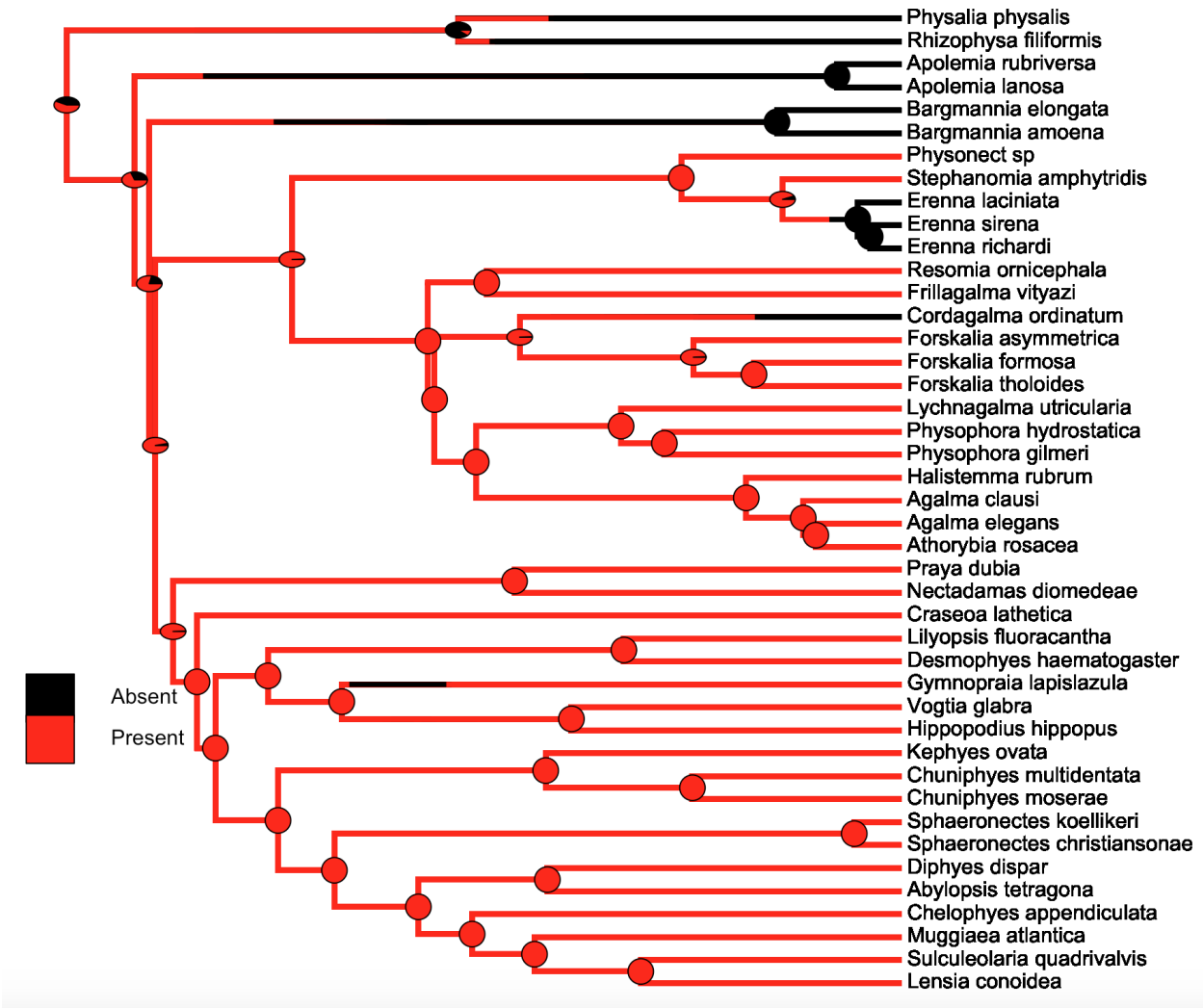


Figure 25: SIMMAP Actively discharging cnidobands presence/absence.



Figure 26: SIMMAP Elastic strands presence/absence.

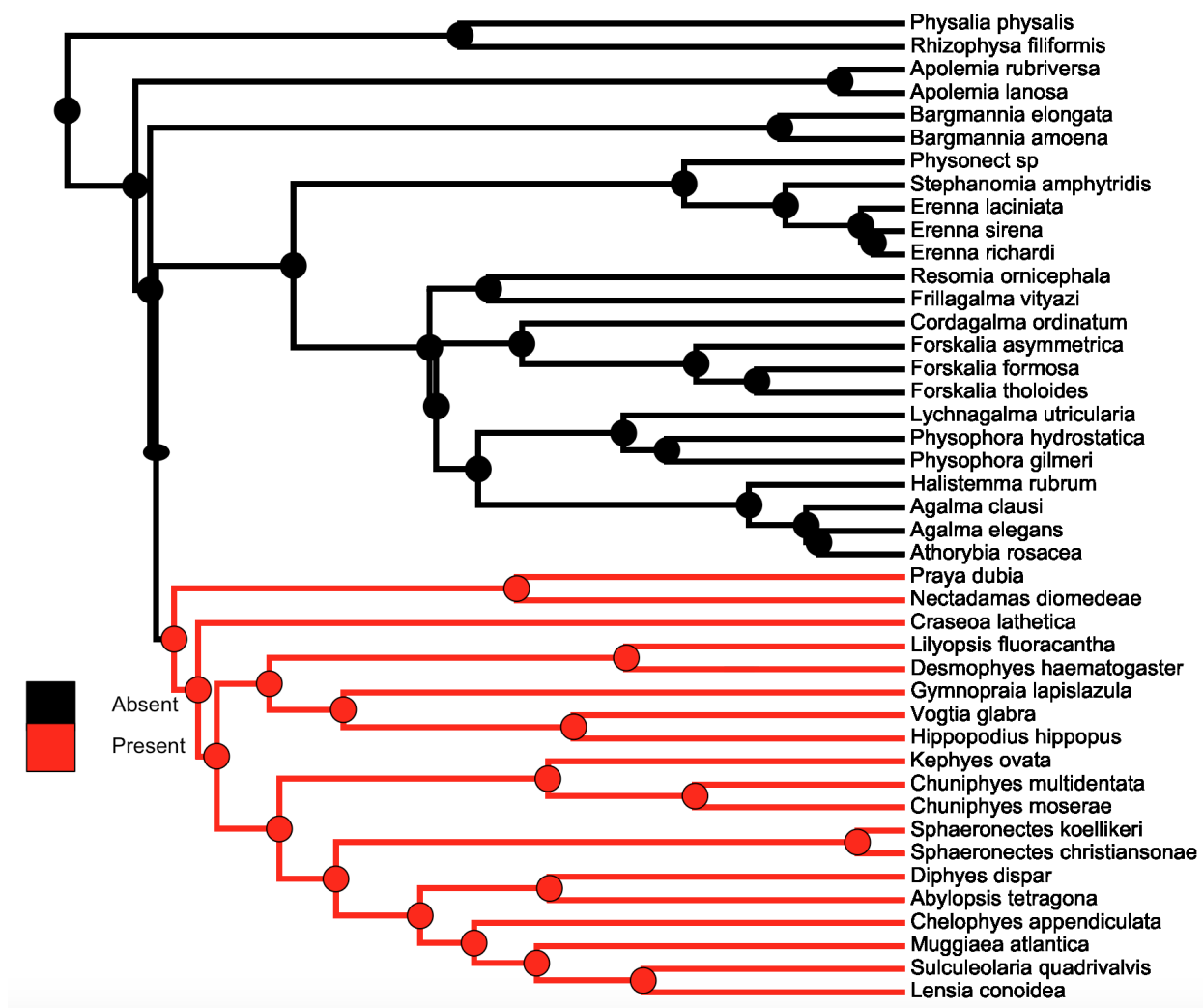


Figure 27: SIMMAP Cnidoband distal desmonemes presence/absence.

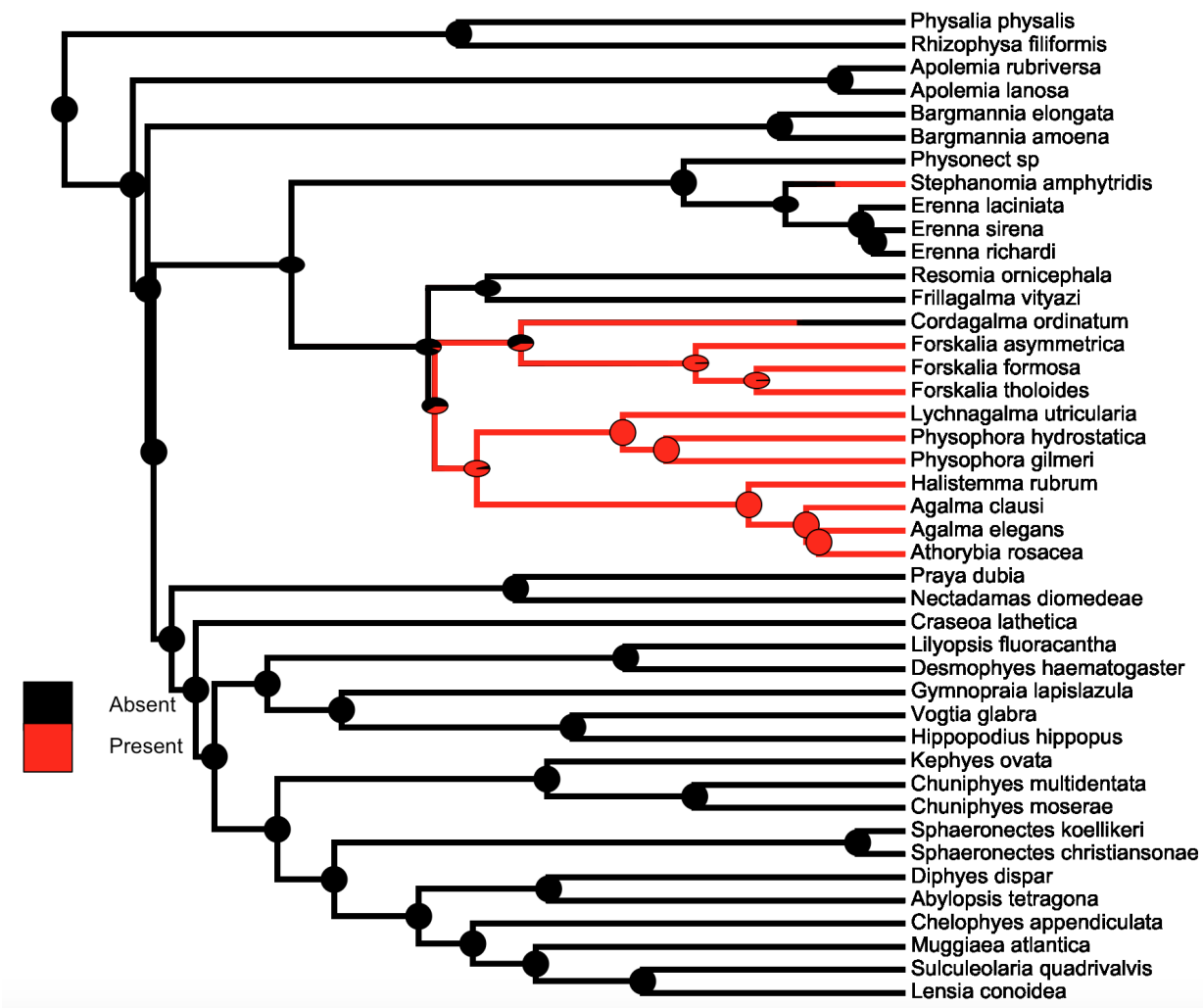


Figure 28: SIMMAP Coiled cnidoaband phenotype presence/absence.

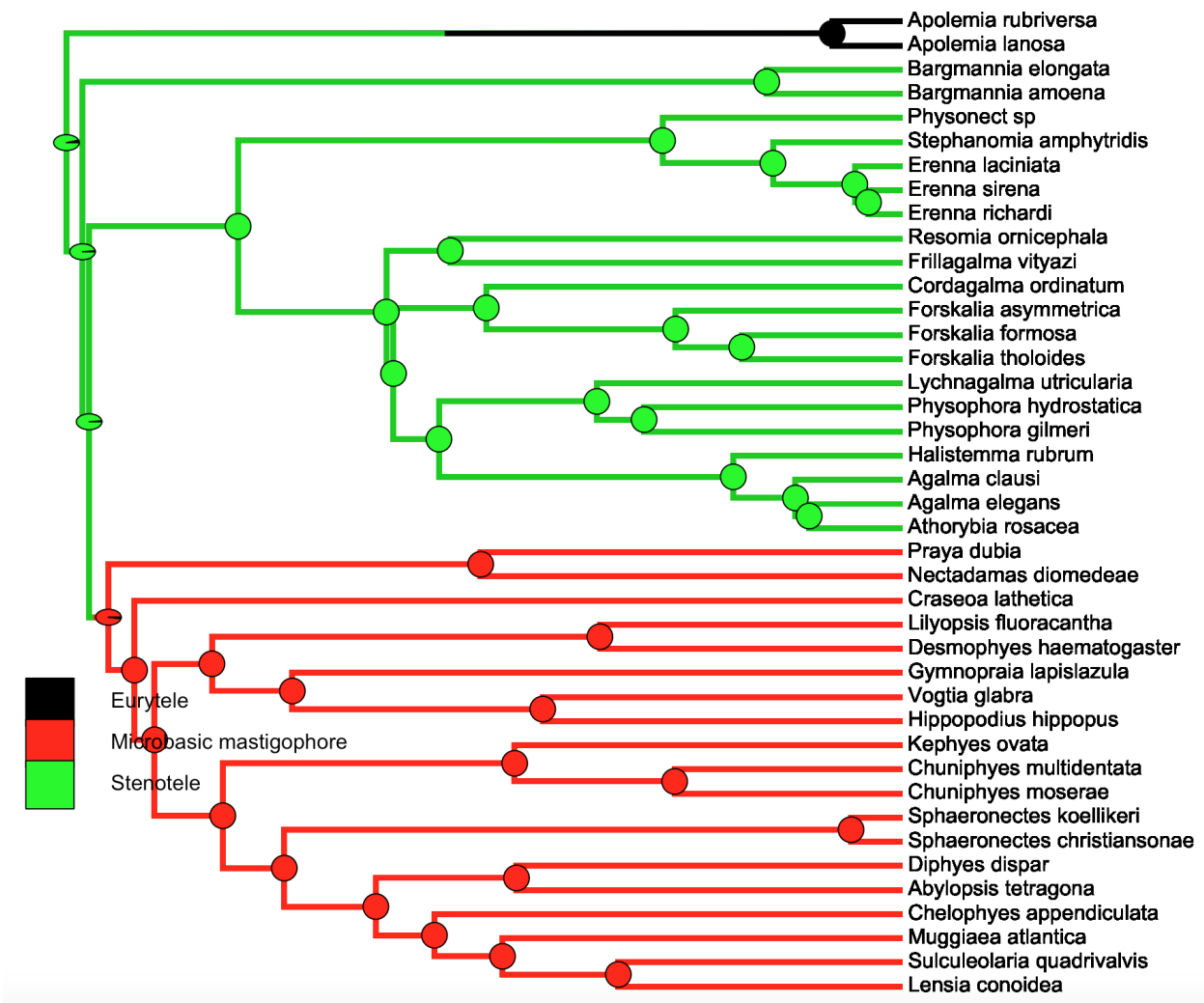


Figure 29: SIMMAP Heteroneme type.

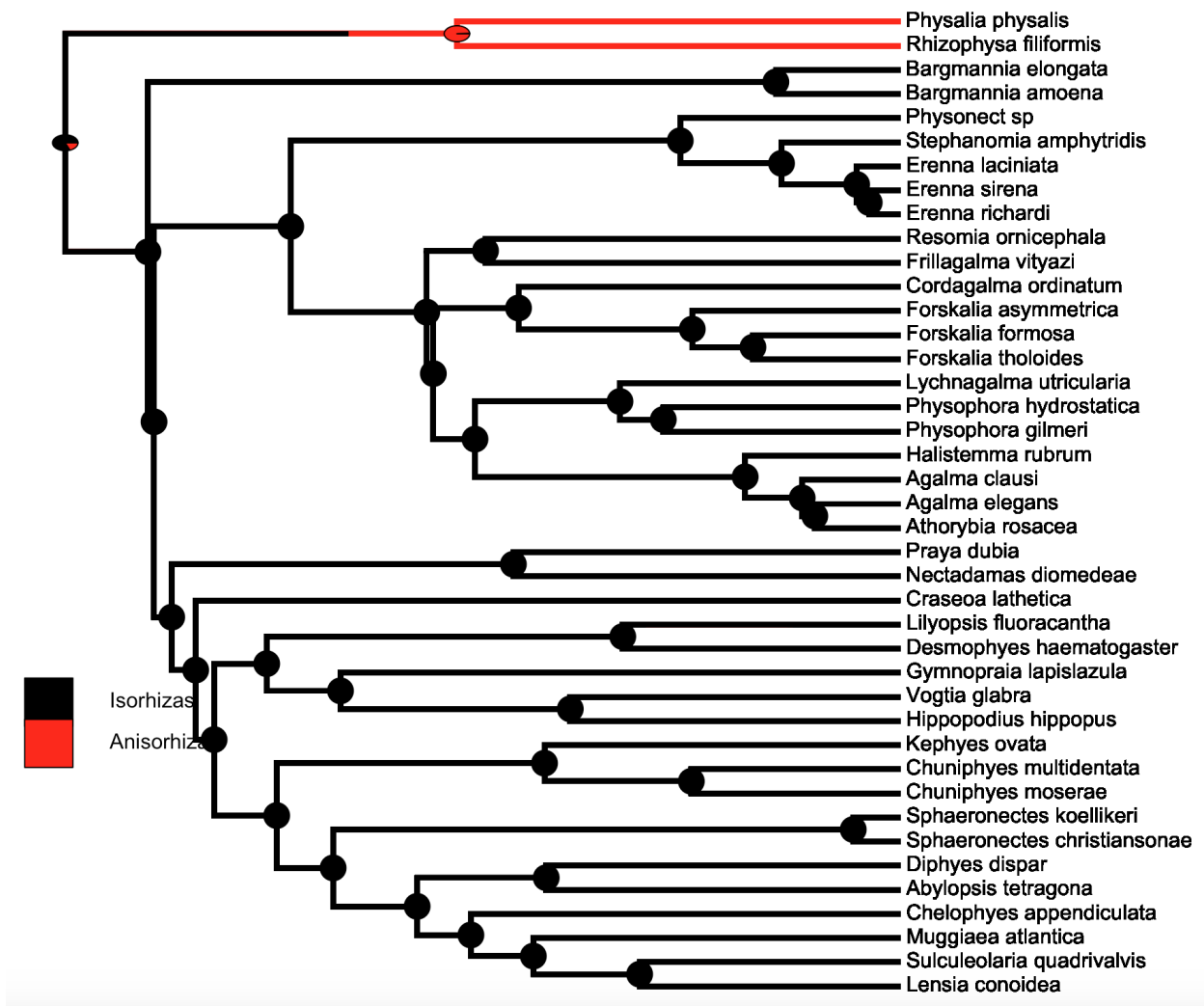


Figure 30: SIMMAP Haplotype type.

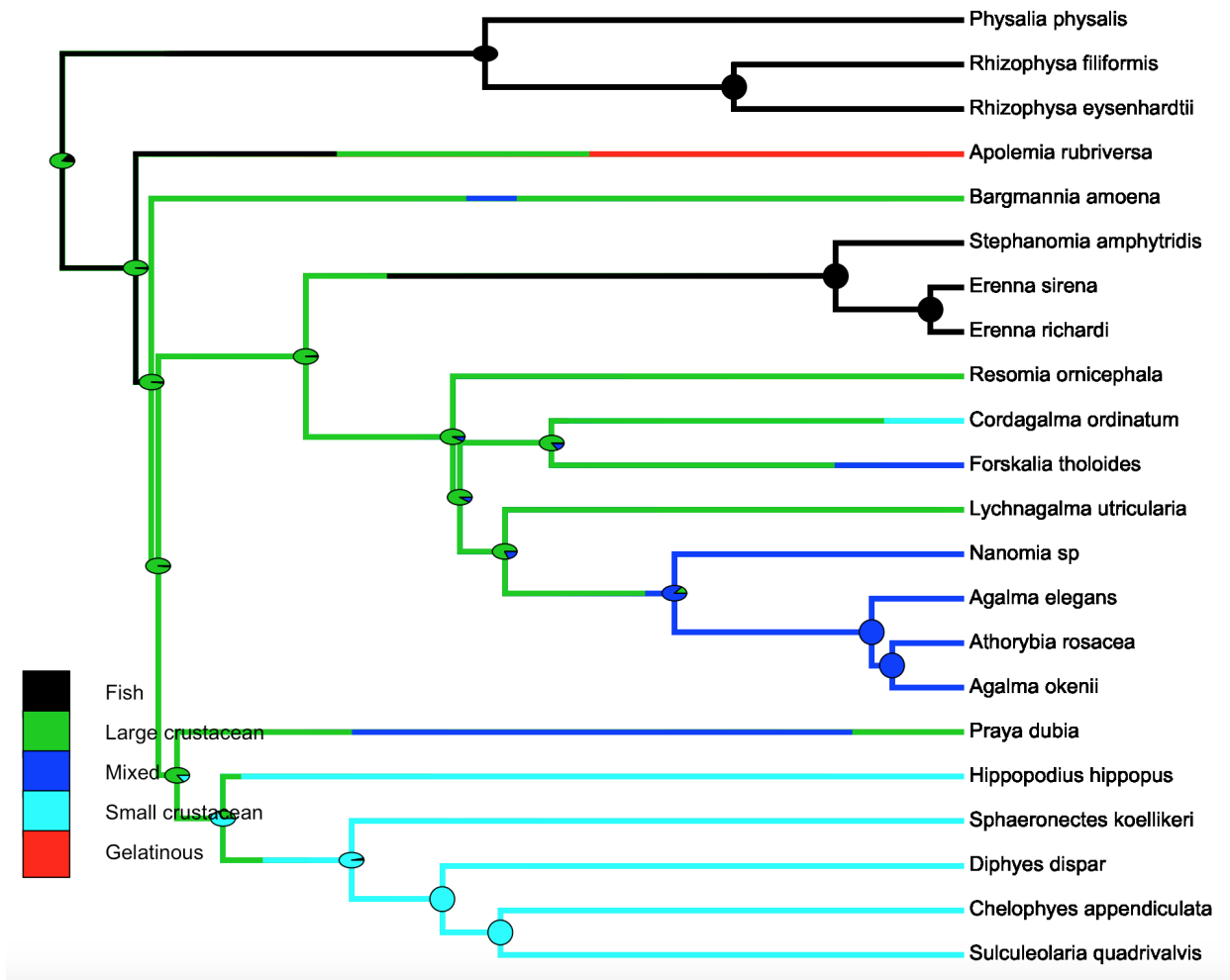


Figure 31: SIMMAP Feeding guilds.

¹³⁹

Bayesian Analysis of Macroevolutionary Mixtures (BAMM) results:

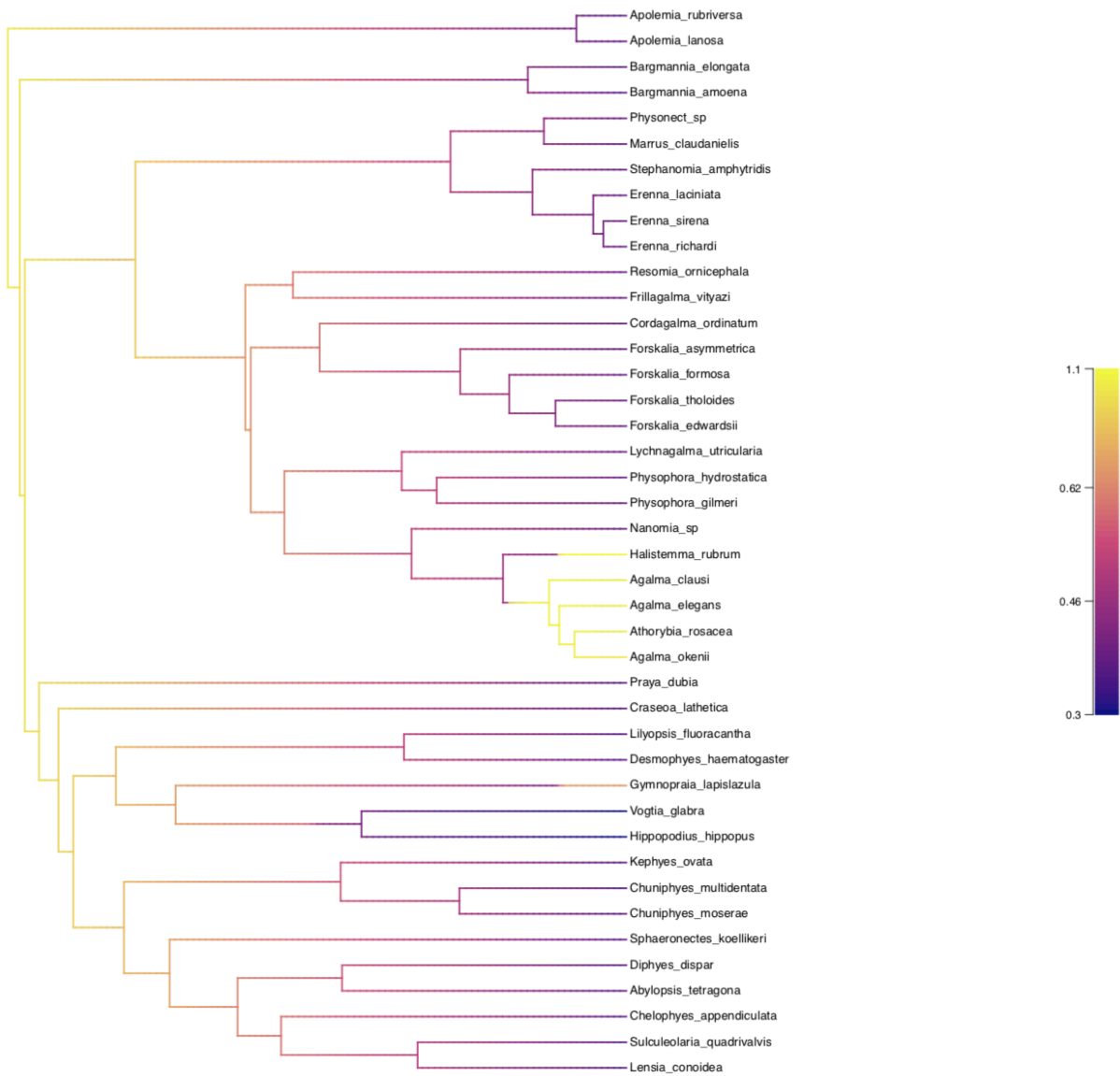


Figure 32: Siphonophore ultrametric tree with estimated trait diversification rates of heteroneme elongation, estimated by BAMM. Yellow = Rate acceleration. Purple = Rate slowdown.

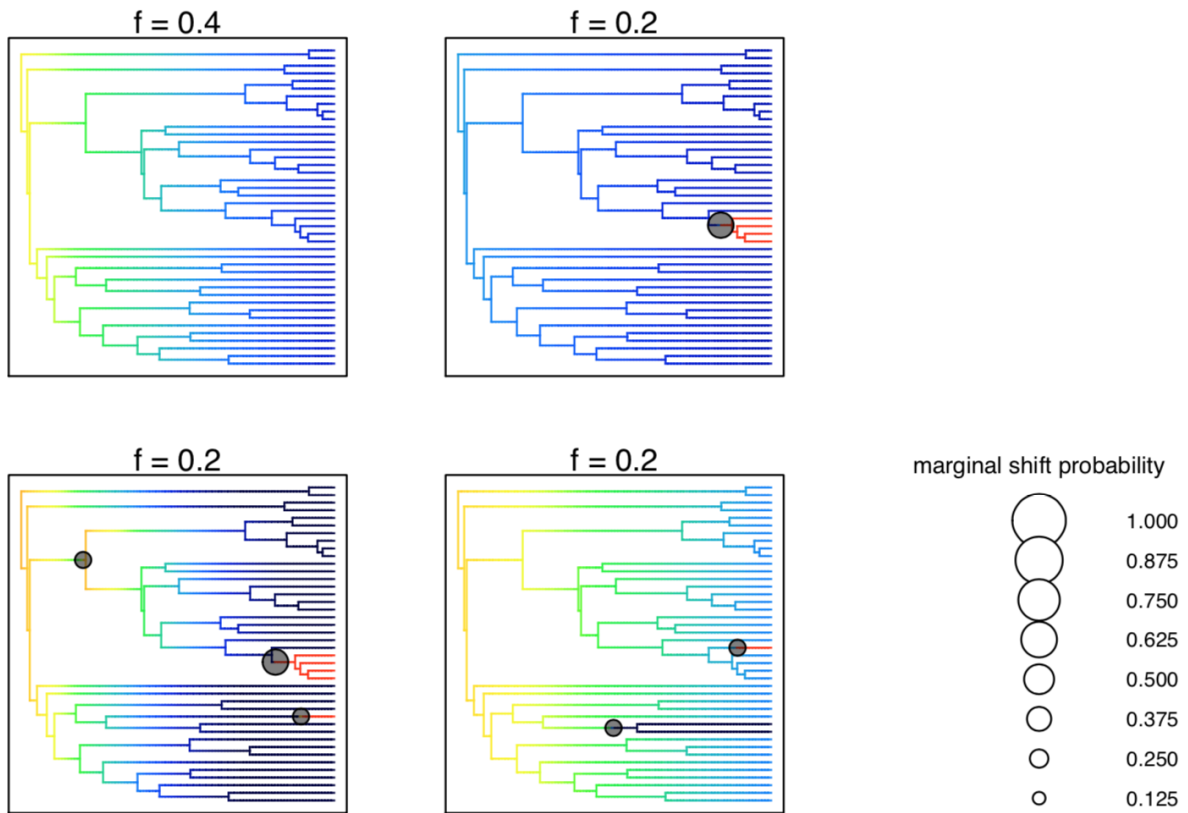


Figure 33: Bayesian 95% credible rate regime shift set for heteroneme elongation. Red = rate acceleration. Blue = rate slowdown. f values are the fraction of the probability of the data accounted for.

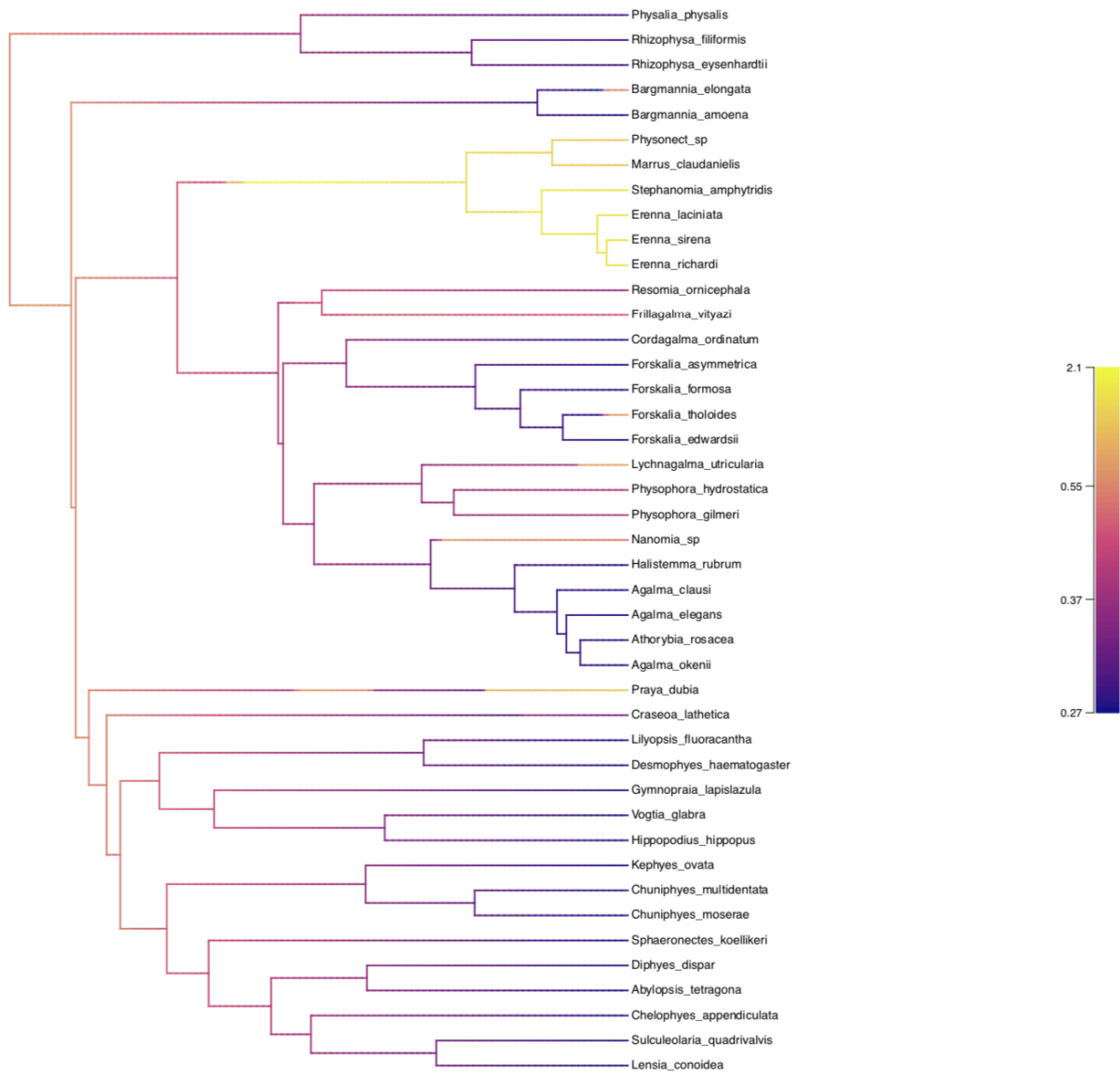


Figure 34: Siphonophore ultrametric tree with estimated trait diversification rates of haploneme elongation, estimated by BAMM. Yellow = Rate acceleration. Purple = Rate slowdown.

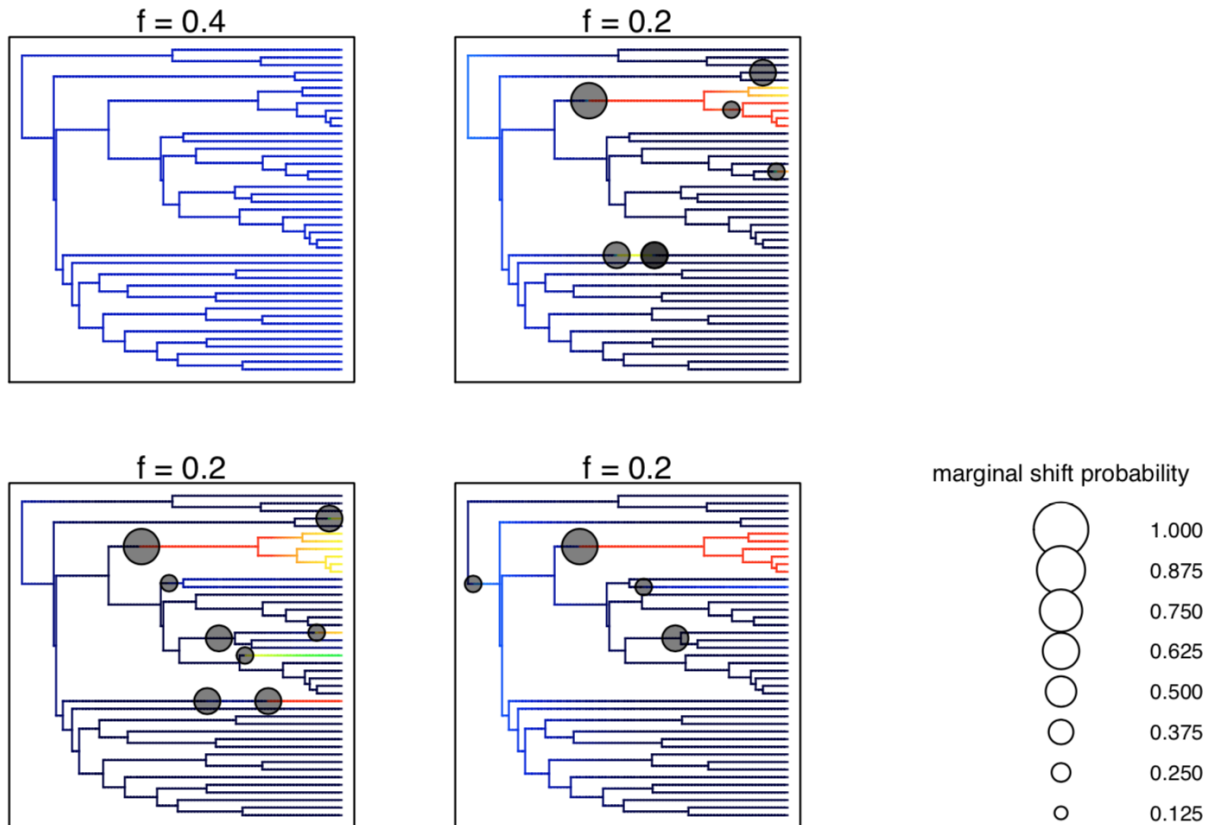
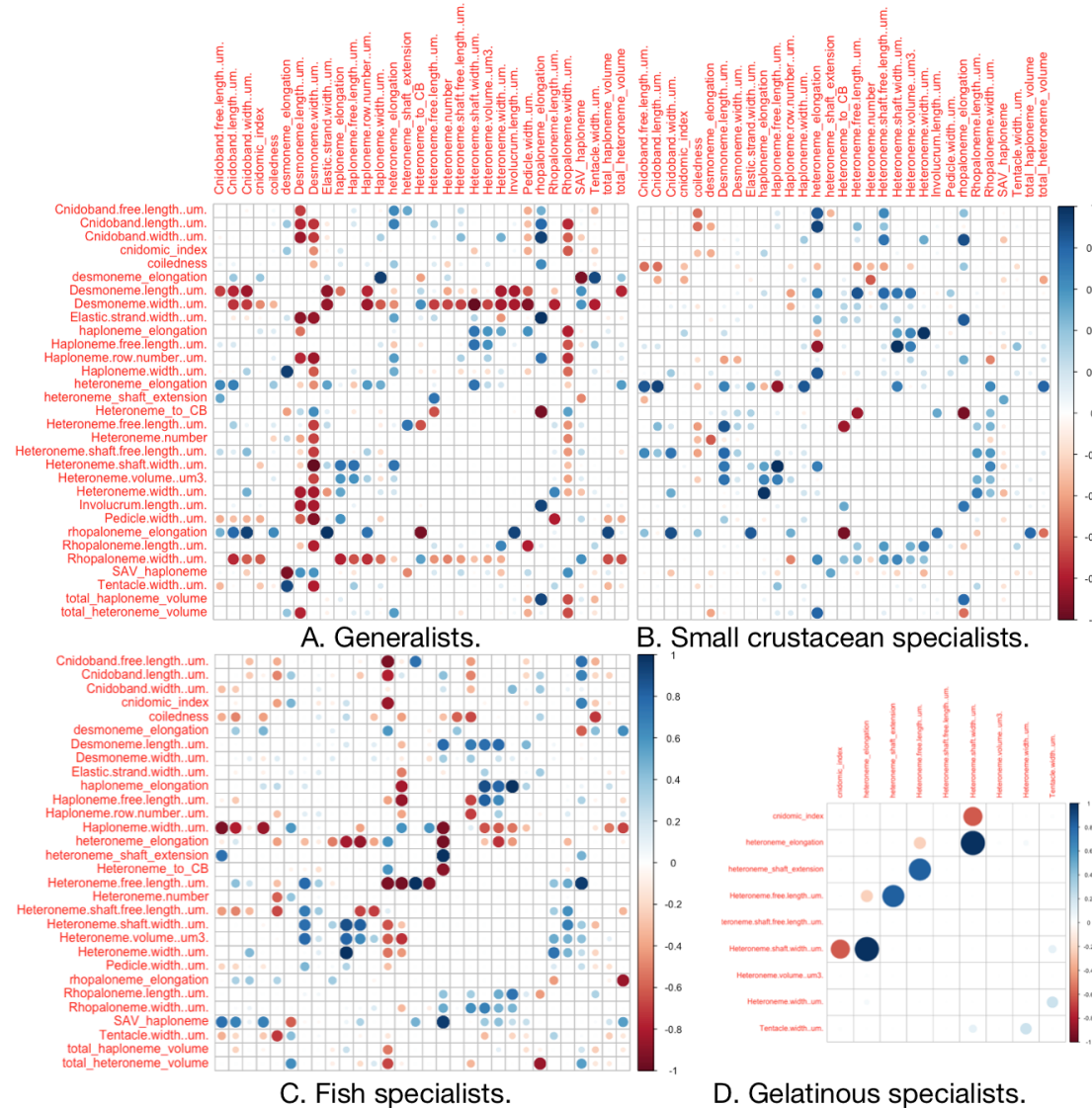


Figure 35: Bayesian 95% credible rate regime shift set for haploneme elongation. Red = rate acceleration. Blue = rate slowdown. f values are the fraction of the probability of the data accounted for.

Variance-Covariance Matrix analyses of phenotypic intergation and evolutionary modularity:

141



143 References

- 144 Bardi J., Marques A.C. 2007. Taxonomic redescription of the portuguese man-of-war, physalia physalis (cnidaria, hydrozoa, siphonophorae, cystonectae) from brazil. Iheringia. 145 Série Zoologia. 97:425–433.
- 146 Blyth C.R. 1972. On simpson's paradox and the sure-thing principle. Journal of the American Statistical Association. 67:364–366.

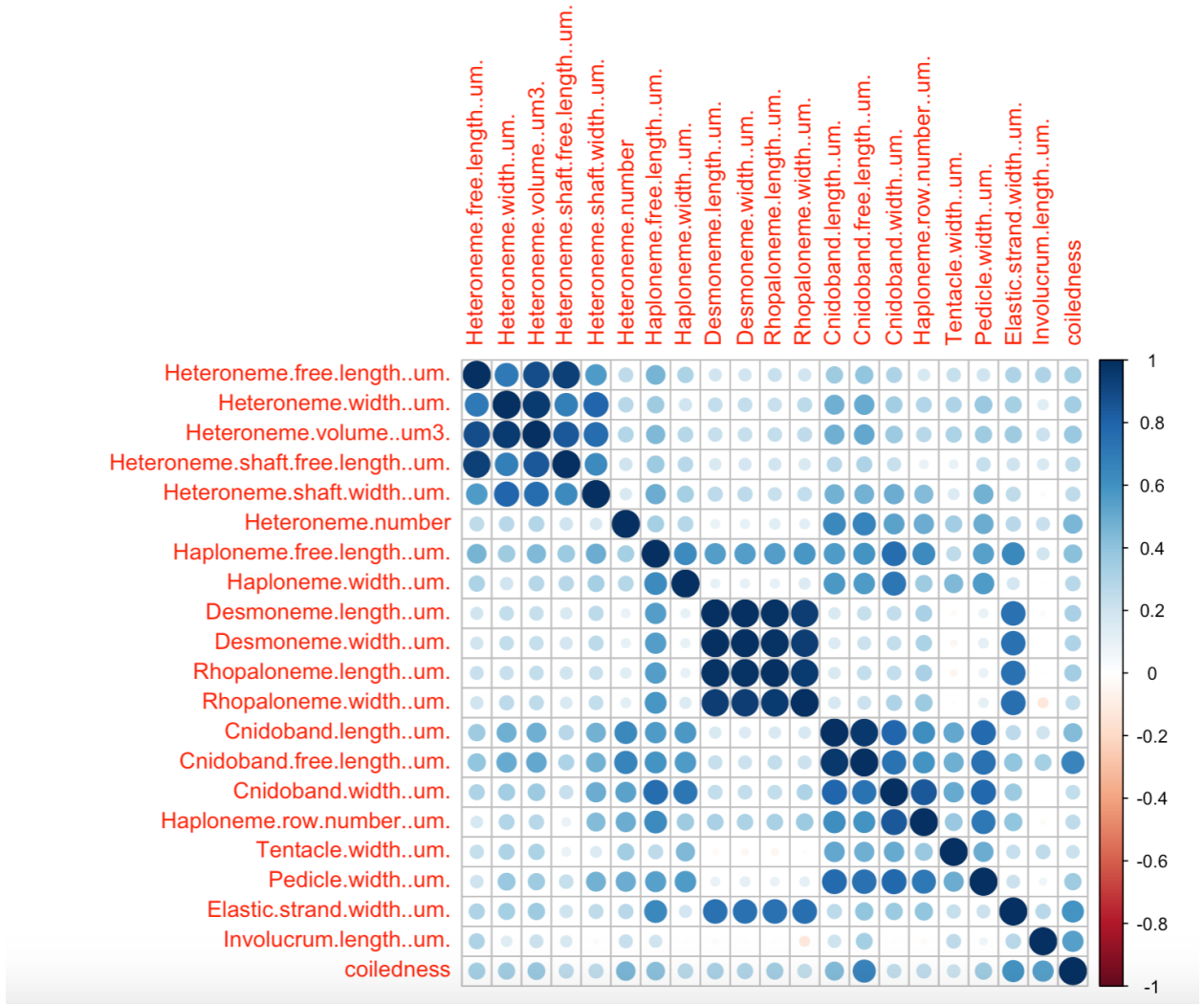


Figure 36: Rate covariance matrix for the whole tree using all taxa (45 species), transforming inapplicable states to zeroes. Covariances scaled to correlations. All characters estimated simultaneously under Brownian Motion.

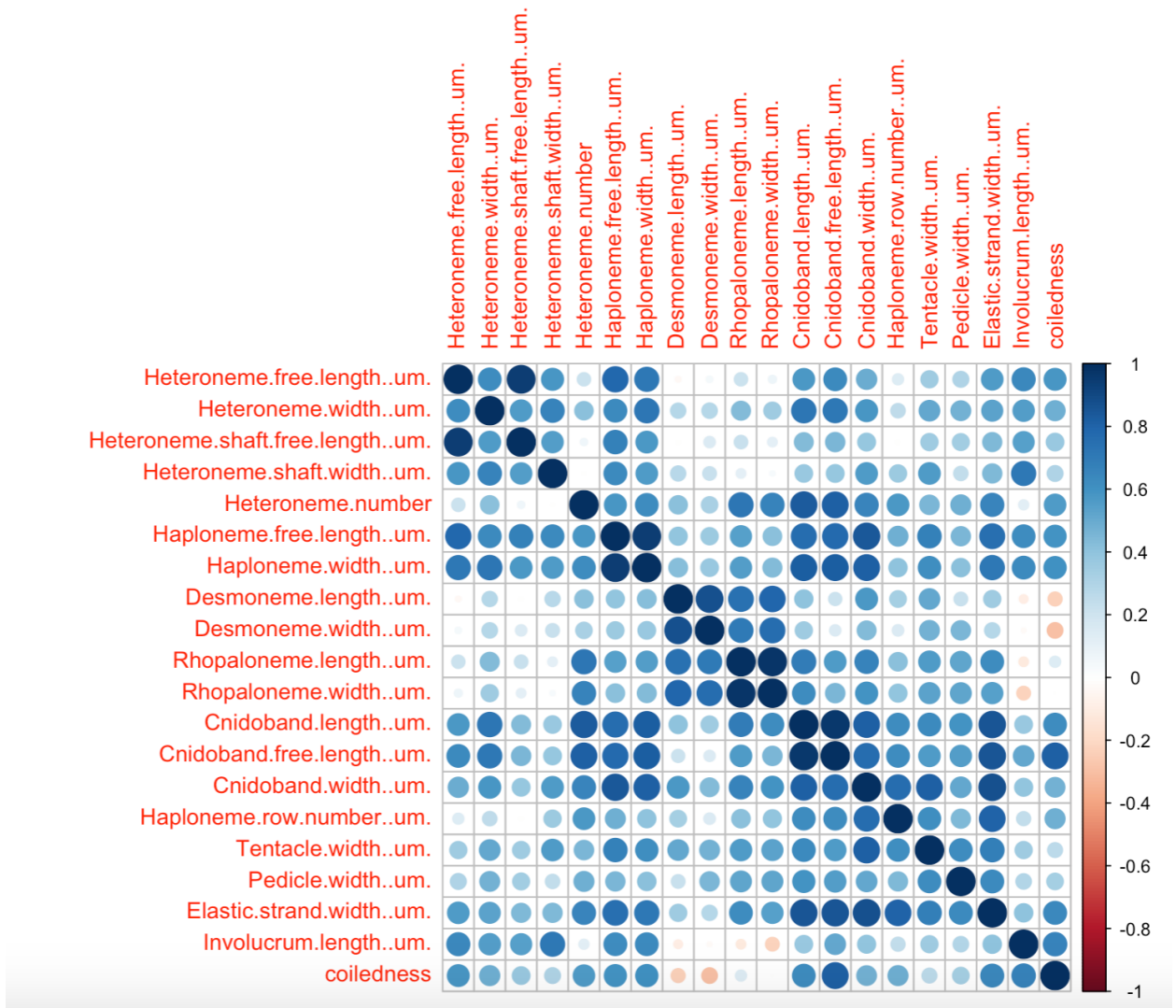


Figure 37: Rate covariance matrix for the whole tree using only taxa without inapplicable states (24 species). Covariances scaled to correlations. All characters estimated simultaneously under Brownian Motion.

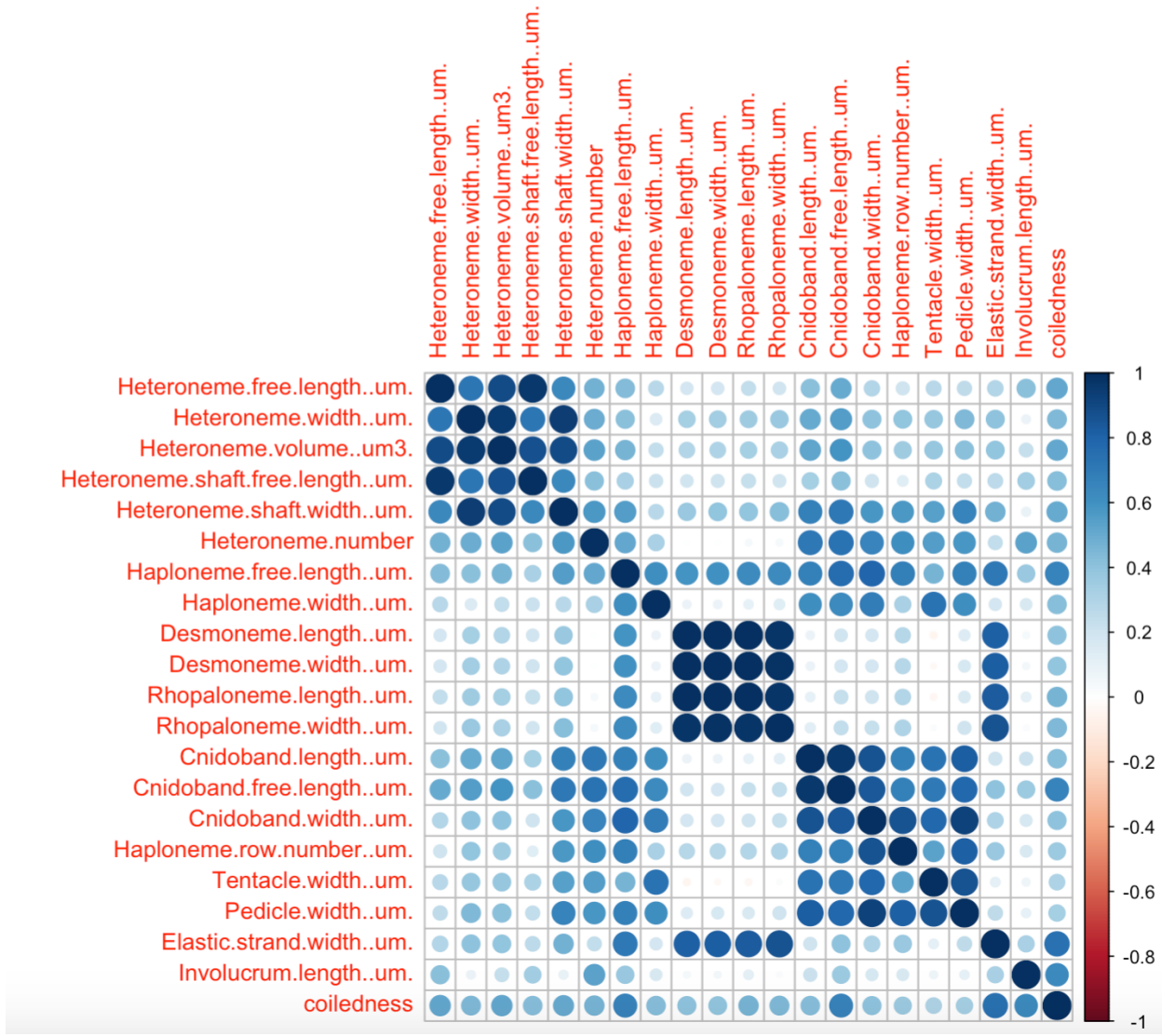


Figure 38: Rate covariance matrix for the whole tree using only taxa with diet data (22 species), transforming inapplicable states to zeroes. Covariances scaled to correlations. All characters estimated simultaneously under Brownian Motion.

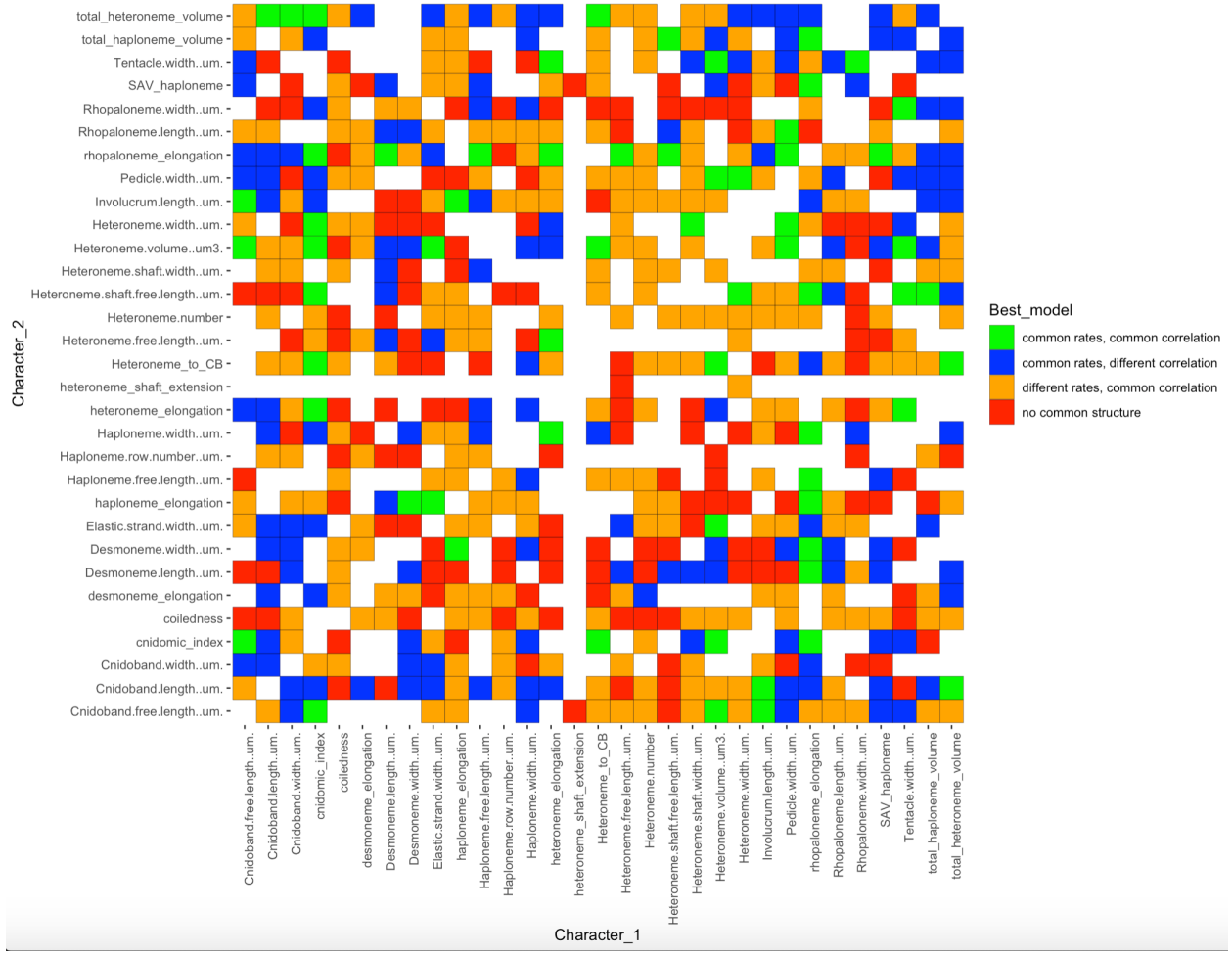


Figure 39: Best models (lowest AIC) supported in a pairwise character rate covariance analysis comparing correlated Brownian Motion models across the five selective regimes. Selective regimes were mapped onto the tree using an ancestral state reconstruction of the feeding guilds. Blank cells represent computationally singular contrasts.

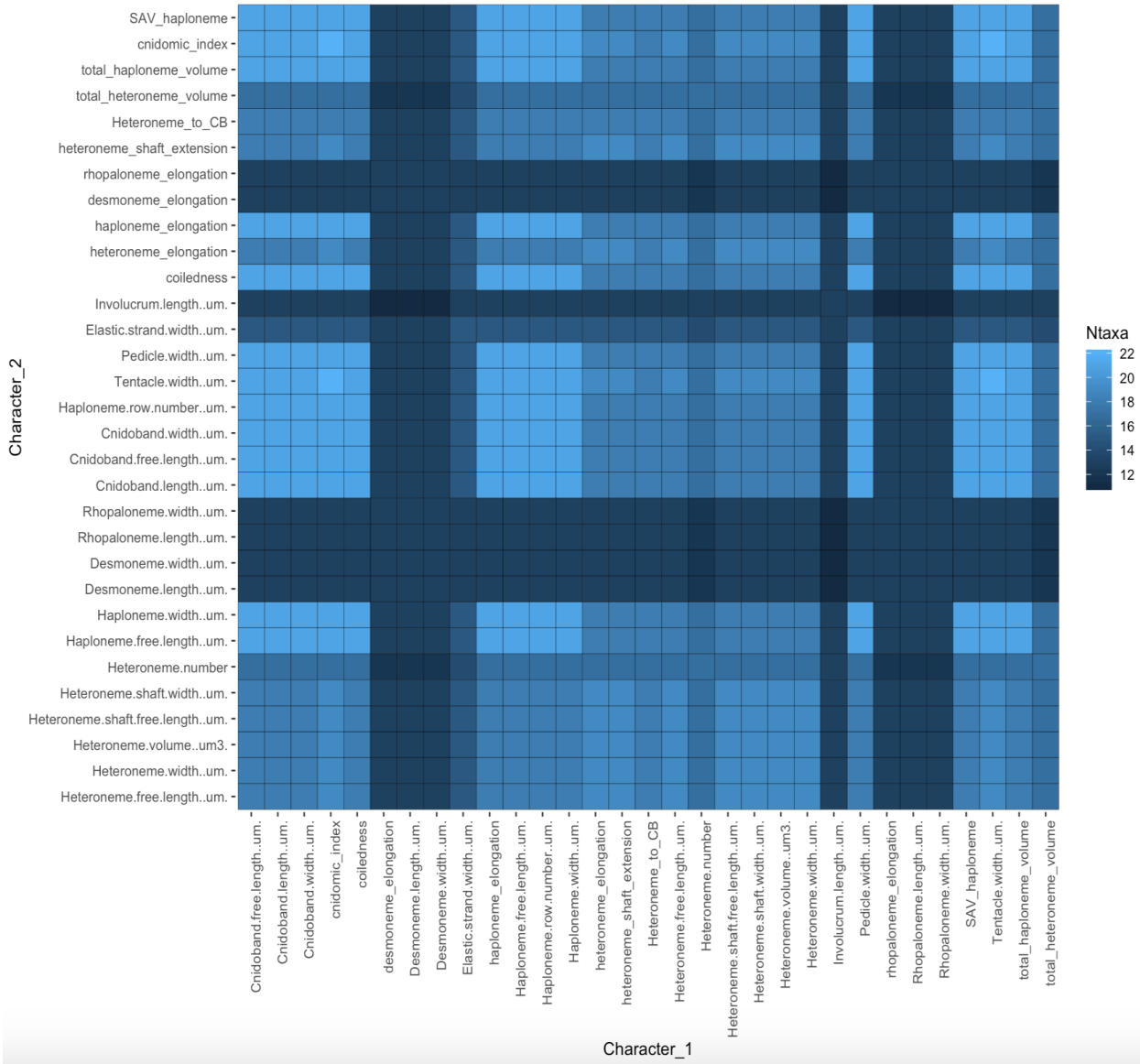


Figure 40: Number of taxa used for each pairwise contrast in the VCV analyses, given the number of taxa without inapplicable states.



Figure 41: Pairwise estimated rate covariance matrices across the five selective regimes, using only taxa with diet data. Covariances scaled to correlations. Selective regimes were mapped onto the tree (22 species with diet data) using a stochastic mapping of the feeding guilds. Tree is pruned to taxa with no inapplicable states for a given character pair. Not all regimes are represented in all contrasts. Question marks represent computationally singular contrasts.

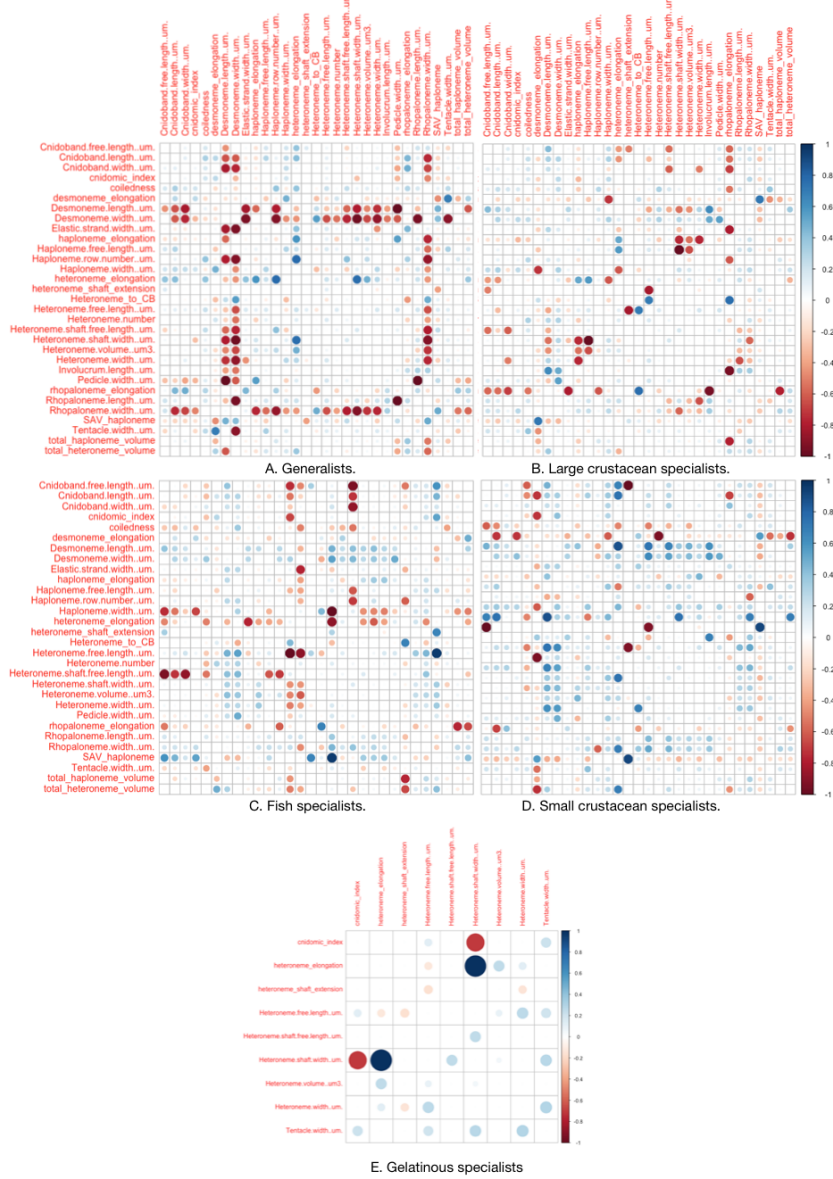


Figure 42: Scaled differences between the regime-specific covariance matrices in @ref{VCV_Regimes} and the whole tree covariance matrix.

- ¹⁴⁹ Felsenstein J. 1985. Phylogenies and the comparative method. *The American Naturalist*.
¹⁵⁰ 125:1–15.
- ¹⁵¹ Jombart T., Devillard S., Balloux F. 2010. Discriminant analysis of principal components:
¹⁵² A new method for the analysis of genetically structured populations. *BMC genetics*. 11:94.
- ¹⁵³ Mitra A. 2009. Are closure terms appropriate or necessary descriptors of zooplankton loss
¹⁵⁴ in nutrient–phytoplankton–zooplankton type models? *Ecological Modelling*. 220:611–620.
- ¹⁵⁵ Munro C., Siebert S., Zapata F., Howison M., Serrano A.D., Church S.H., Goetz F.E.,
¹⁵⁶ Pugh P.R., Haddock S.H., Dunn C.W. 2018. Improved phylogenetic resolution within
¹⁵⁷ siphonophora (cnidaria) with implications for trait evolution. *Molecular Phylogenetics and*
¹⁵⁸ *Evolution*.
- ¹⁵⁹ Pugh P., Baxter E. 2014. A review of the physonect siphonophore genera halistemma
¹⁶⁰ (family agalmatidae) and stephanomia (family stephanomiidae). *Zootaxa*. 3897:1–111.
- ¹⁶¹ Revell L.J. 2012. Phytools: An r package for phylogenetic comparative biology (and other
¹⁶² things). *Methods in Ecology and Evolution*. 3:217–223.
- ¹⁶³ Revell L.J., Chamberlain S.A. 2014. Rphylip: An r interface for phylip. *Methods in*
¹⁶⁴ *Ecology and Evolution*. 5:976–981.
- ¹⁶⁵ Simpson G.G. 1955. Major features of evolution. Columbia University Press: New York.
- ¹⁶⁶ Totton A.K., Bargmann H.E. 1965. A synopsis of the siphonophora. *British Museum*
¹⁶⁷ (Natural History).
- ¹⁶⁸ Uyeda J.C., Zenil-Ferguson R., Pennell M.W. 2018. Rethinking phylogenetic comparative
¹⁶⁹ methods. *Systematic Biology*. 67:1091–1109.